

1 Measurement report: Firework impacts on air quality in Metro Manila, Philippines during the  
2 2019 New Year revelry

3 Genevieve Rose Lorenzo<sup>1,2</sup>, Paola Angela Bañaga<sup>2,3</sup>, Maria Obiminda Cambaliza<sup>2,3</sup>, Melliza  
4 Templonuevo Cruz<sup>3,4</sup>, Mojtaba AzadiAghdam<sup>6</sup>, Avelino Arellano<sup>1</sup>, Grace Betito<sup>3</sup>, Rachel  
5 Braun<sup>6</sup>, Andrea F. Corral<sup>6</sup>, Hossein Dadashazar<sup>6</sup>, Eva-Lou Edwards<sup>6</sup>, Edwin Eloranta<sup>5</sup>, Robert  
6 Holz<sup>5</sup>, Gabrielle Leung<sup>2</sup>, Lin Ma<sup>6</sup>, Alexander B. MacDonald<sup>6</sup>, James Bernard Simpas<sup>2,3</sup>, Connor  
7 Stahl<sup>6</sup>, Shane Marie Visaga<sup>2,3</sup>, Armin Sorooshian<sup>1,6</sup>

8 <sup>1</sup>Department of Hydrology and Atmospheric Sciences, University of Arizona, Tucson, Arizona,  
9 85721, USA

10 <sup>2</sup>Manila Observatory, Quezon City, 1108, Philippines

11 <sup>3</sup>Department of Physics, School of Science and Engineering, Ateneo de Manila University,  
12 Quezon City, 1108, Philippines

13 <sup>4</sup>Institute of Environmental Science and Meteorology, University of the Philippines, Diliman,  
14 Quezon City, 1101, Philippines

15 <sup>5</sup>Space Science and Engineering Center, University of Wisconsin - Madison, Madison,  
16 Wisconsin, 53706, USA

17 <sup>6</sup>Department of Chemical and Environmental Engineering, University of Arizona, Tucson,  
18 Arizona, 85721, USA

19 *Correspondence to: armin@email.arizona.edu*

## 20 Abstract

21 Fireworks degrade air quality, reduce visibility, alter atmospheric chemistry, and cause short-  
22 term adverse health effects. However, there have not been any comprehensive physicochemical  
23 and optical measurements of fireworks and their associated impacts in a Southeast Asia  
24 megacity, where fireworks are a regular part of the culture. Size-resolved particulate matter (PM)  
25 measurements were made before, during, and after New Year 2019 at the Manila Observatory in  
26 Quezon City, Philippines, as part of the Cloud, Aerosol, and Monsoon Processes Philippines  
27 Experiment (CAMP<sup>2</sup>Ex). A High Spectral Resolution Lidar (HSRL) recorded a substantial  
28 increase in backscattered signal associated with high aerosol loading ~440 m above the surface  
29 during the peak of firework activities around 00:00 (local time). This was accompanied by PM<sub>2.5</sub>  
30 concentrations peaking at 383.9  $\mu\text{g m}^{-3}$ . During the firework event, water-soluble ions and  
31 elements, which affect particle formation, growth, and fate, were mostly in the submicrometer  
32 diameter range. Total ( $> 0.056 \mu\text{m}$ ) water-soluble bulk particle mass concentrations were  
33 enriched by 5.7 times during the fireworks relative to the background (i.e., average of before and  
34 after the firework). The water-soluble mass fraction of PM<sub>2.5</sub> increased by 18.5% above that of  
35 background values. This corresponded to increased volume fractions of inorganics which  
36 increased bulk particle hygroscopicity, kappa ( $\kappa$ ), from 0.11 (background) to 0.18 (fireworks).  
37 Potassium and non-sea salt (nss)  $\text{SO}_4^{2-}$  contributed the most (70.9%) to the water-soluble mass,  
38 with their mass size distributions shifting from a smaller to a larger submicrometer mode during  
39 the firework event. On the other hand, mass size distributions for  $\text{NO}_3^-$ ,  $\text{Cl}^-$ , and  $\text{Mg}^{2+}$  (21.1%  
40 mass contribution) shifted from a supermicrometer mode to a submicrometer mode. Being both  
41 uninfluenced by secondary aerosol formation and constituents of firework materials, a subset of  
42 species were identified as the best firework tracer species (Cu, Ba, Sr,  $\text{K}^+$ , Al, and Pb). Although  
43 these species (excluding  $\text{K}^+$ ) only contributed 2.1% of the total mass concentration of water-  
44 soluble ions and elements, they exhibited the highest enrichments (6.1 to 65.2) during the  
45 fireworks. Surface microscopy analysis confirmed the presence of potassium/chloride-rich cubic  
46 particles along with capsule-shaped particles in firework samples. The results of this study  
47 highlight how firework emissions change the physicochemical and optical properties of water-  
48 soluble particles (e.g., mass size distribution, composition, hygroscopicity, and aerosol  
49 backscatter), which subsequently alters the background aerosol's respirability, influence on  
50 surroundings, ability to uptake gases, and viability as cloud condensation nuclei (CCN).

## 51 1. Introduction

52 Fireworks affect local populations through visibility reduction and increased health risks due to  
53 briefly elevated particulate matter (PM) levels. Total PM mass concentrations during local  
54 celebrations in the following cities exceeded the 24 h U.S. National Ambient Air Quality  
55 Standard (NAAQS) for PM<sub>10</sub> of 150 µg m<sup>-3</sup>: Leipzig, Germany, (Wehner et al., 2000), Texas,  
56 United States [U.S.], (Karnae, 2005), Montreal, Canada (Joly et al., 2010), and New Delhi, India,  
57 (Mönkkönen et al., 2004). Firework emissions from at least nineteen studies have also been  
58 linked to exceedance of the 24 h U.S. NAAQS limit for PM<sub>2.5</sub> of 35 µg m<sup>-3</sup> (Lin, 2016 and  
59 references therein). Higher PM concentrations from fireworks have been reported more  
60 frequently in Asia (i.e., India, China, and Taiwan) compared to Western countries (Lin, 2016;  
61 Sarkar et al., 2010).

62 Health effects are of major concern during firework periods based on both short and long-term  
63 exposure. For example, Diwali is a major firework festival in India, and it was shown that  
64 chronic exposure to three of the most prominent tracer species (Sr, K, and Ba) translated to a 2%  
65 increase in health effects based on the non-carcinogenic hazard index (Sarkar et al., 2010). On  
66 the other hand, short term exposure to firework pollutants increases asthma risk, eye allergies,  
67 cardiovascular and pulmonary issues, cough, and fever (Moreno et al., 2010; Singh et al., 2019;  
68 Barman et al., 2008; Becker et al., 2000; Beig et al., 2013; Hirai et al., 2000). Firework pollutants  
69 also impact clouds and the hydrological cycle, owing to associated aerosols serving as cloud  
70 condensation nuclei (CCN) (Drewnick et al., 2006) and subsequently impacting surface  
71 ecosystems after wet deposition (Wilkin et al., 2007). Although fireworks emit particles with  
72 various sizes into the atmosphere, fine particles associated with PM<sub>2.5</sub> are most relevant to public  
73 health effects, scattering efficiency, and CCN activation (Vecchi et al., 2008; Perry, 1999).  
74 Knowing the various effects of firework emissions depends on knowing their physical, chemical,  
75 and optical properties.

76 Measurements of the chemical composition of firework emissions are important in order to  
77 understand how they affect local air quality. The main components of fireworks are fuels (metals  
78 and alloys, metalloids, and non-metals), oxidizers (nitrates, perchlorates, and chlorates), and  
79 coloring agents (metal salts) (Steinhauser and Klapotke, 2010). Previous studies have relied on  
80 tracer species to establish confidence in distinguishing the firework source from background air  
81 and other sources (Sarkar et al., 2010). Potassium historically has been the most observable  
82 tracer for fireworks emissions (Wang et al., 2007; Drewnick et al., 2006; Perry, 1999), with  
83 concentrations reaching 58 µg m<sup>-3</sup> during the Diwali Festival in India (Kulshrestha et al., 2004).  
84 Firework color is created by metal salts such as Sr for red, Ba for green, and Cu for blue-violet,  
85 all three of which have and have been found to be effective tracers of fireworks (Walsh et al.,  
86 2009; Vecchi et al., 2008). Strontium in particular is an indicator of the spatial and temporal  
87 extent of firework smoke plumes (Perry, 1999) because of the high prevalence of red in  
88 fireworks and it is not affected by traffic emissions (Moreno et al., 2010). Other components  
89 measured in the air that have been attributed to fireworks include metals (Al, Cd, Cu, Ti, Mg,  
90 Mn, Ni, Zn, As, Bi, Co, Ga, Hg, Cr, Pb, Rb, Sb, P, Tl, Ag) and their salt anion counterparts (S, P,  
91 Cl). Thallium makes a green flame. Potassium and Ag (as AgCNO or silver fulminate) are  
92 propellants, Al is fuel, and Pb provides steady burn and is also used as an igniter for firework

93 explosions. Chromium is a catalyst for propellants, Mg is a fuel, and  $Mg^{2+}$  is a neutralizer or  
94 oxygen donor (U.S. Department of Transportation, 2013). Manganese is either a fuel or oxidizer,  
95 and Zn is used for sparks (Licudine et al., 2012; Martín-Alberca and García-Ruiz, 2014;  
96 Shimizu, 1988; Wang et al., 2007; Ennis and Shanley, 1991). Also from fuel and oxidizer  
97 combustion are species such as  $NO_3^-$ ,  $SO_4^{2-}$ , and organics including oxaloacetic acid (Alpert and  
98 Hopke, 1981; Barman et al., 2008; Carranza et al., 2001; Dorado et al., 2001; Drewnick et al.,  
99 2006; Joly et al., 2010; Joshi et al., 2016; Kulshrestha et al., 2004; Kumar et al., 2016; Lin et al.,  
100 2016; Moreno et al., 2010; Sarkar et al., 2010; Tanda et al., 2019; Thakur et al., 2010; Joshi et  
101 al., 2019). Firework-derived chloride in Taiwan has been attributed to raw materials such as  
102  $KClO_3$ ,  $ClO_3$ , and  $ClO_4$  with  $Cl^-:Na^+$  ratios reaching approximately 3 (Tsai et al., 2012). Black  
103 carbon mass concentrations during firework events can either increase due to firework emissions  
104 or decrease owing to fewer vehicles on the road (Kumar et al., 2016; Yadav et al., 2019). In both  
105 cases, the black carbon mass fraction decreases due to a greater contribution of other constituents  
106 in firework emissions. Organic mass concentrations and mass fractions have been noted to  
107 increase and decrease, respectively, with fireworks (Zhang et al., 2019). Governed largely by  
108 composition, particulate hygroscopicity and solubility have also been found to be altered by  
109 fireworks depending on the emitted species. Inorganic salts ( $K_2SO_4$ ,  $KCl$ ) dominated the aerosol  
110 hygroscopicity in Xi'an, China during fireworks (Wu et al., 2018). In the Netherlands,  
111 enhancements in salt mixtures containing  $SO_4^{2-}$ ,  $Cl^-$ ,  $Mg^{2+}$ , and  $K^+$  were noted to enhance  
112 hygroscopicity (ten Brink et al., 2018). Copper and Mg were observed to become more soluble in  
113 firework emissions in Delhi, India, while Mn, As, Ba, and Pb became less soluble (Perrino et al.,  
114 2011). The water-soluble aerosol component from fireworks in Sichuan Basin (China) were  
115 internally mixed and enhanced the hygroscopicity of submicrometer aerosols, especially the  
116 larger particles (Yuan et al., 2020).

117 In addition to composition, a necessary aspect of characterizing impacts of firework emissions is  
118 to measure aerosol size distributions within the short timeframe of an event (Joshi et al., 2019).  
119 Owing to combustion during firework events, PM concentrations are dominated by particles in  
120 the submicrometer range (Vecchi et al., 2008; Nicolás et al., 2009; Joshi et al., 2019; Pirker et  
121 al., 2020; Do et al., 2012). Particle number concentration maxima have been noted for the  
122 nucleation (0.01 to 0.02  $\mu m$ ) and Aitken (0.02 to 0.05  $\mu m$ ) modes (Yadav et al., 2019; Yuan et  
123 al., 2020), in addition to both the small (0.1 to 0.5  $\mu m$ ) (Wehner et al., 2000; Zhang et al., 2010)  
124 and large (0.5 to 1.0  $\mu m$ ) ends of the accumulation mode (Vecchi et al., 2008) during firework  
125 events. In Nanning, China,  $SO_4^{2-}$  peaked at 0.62  $\mu m$  during fireworks (Li et al., 2017). The mass  
126 diameter of  $K^+$  was 0.7  $\mu m$  due to firework emissions after transport in Washington State (Perry,  
127 1999). There are a few studies with observed particle mass concentration increases in the coarser  
128 but still respirable (< 10  $\mu m$ ) mode (Tsai et al., 2011). In terms of dynamic behavior in the size  
129 distributions, past work has shown a shift in number concentration from nucleation and Aitken  
130 modes to the smaller end of the accumulation mode (0.1 to 0.5  $\mu m$ ), due to increased coagulation  
131 sinks (Zhang et al., 2010). Finer temporal scale monitoring has revealed steep increases in  
132 nucleation mode and Aitken mode particle concentrations associated with firework emissions  
133 followed by a growth in accumulation mode particle number concentrations due to coagulation

134 (Yadav et al., 2019). An opposite shift to a smaller size distribution has been observed for certain  
135 species (Mg, Al, Cu, Sr, and Ba) from the coarse mode to accumulation mode (Tanda et al.,  
136 2019). Other work has shown that while there is usually a quick drop in particle concentration to  
137 background values after firework events (Joly et al., 2010), elevated number concentrations of  
138 accumulation mode particles are maintained for up to three hours after peak firework activity  
139 (Hussein et al., 2005). New particle formation events with fireworks have also been reported in  
140 Mumbai, India (Joshi et al., 2016), with enrichments of primary and secondary particles for up to  
141 30 minutes after peak firework activity. Particle aging due to distance from the source and  
142 meteorology alter firework emission particle concentrations (Joly et al., 2010) and size  
143 distributions (Khaparde et al., 2012).

144 Meteorological and dynamic parameters such as wind speed, level of mixing (turbulent kinetic  
145 energy), and mixing layer height (Lai and Brimblecombe, 2020) influence peak concentration  
146 and composition of aerosols after fireworks, as well as particle residence time in the atmosphere  
147 and transport to nearby regions (Vecchi et al., 2008). Although firework activities are episodic,  
148 their particulate emissions, especially in the submicrometer mode (Do et al., 2012), reside in the  
149 atmosphere for as long as several days to weeks (Liu et al., 1997; Lin et al., 2016; Kong et al.,  
150 2015; Do et al., 2012). Dispersion of the particles under low wind speed ( $1 \text{ m s}^{-1}$ ) for particles  
151 between 0.4 and  $1 \mu\text{m}$  is estimated at 12 h (Vecchi et al., 2008) and can reach distances as far as  
152 a hundred kilometers (Perry, 1999). Aitken mode and larger particles are dispersed by wind more  
153 than nucleation-mode particles (Agus et al., 2008). Meteorological conditions, such as rainfall,  
154 can also decrease firework particle loading in the air and relative humidity can change the  
155 hygroscopicity of firework emissions (Hussein et al., 2005), thereby affecting their size and  
156 radiative properties.

157 Studies on aerosol properties are limited for the rapidly developing region of Southeast Asia  
158 (Tsay et al., 2013). This compounds the challenge to understand the interactions between  
159 aerosols and the complex hydro-meteorological and geological environment in Southeast Asia  
160 (Reid et al., 2013). Increased local and transported emissions (Hopke et al., 2008; Oanh et al.,  
161 2006) in Southeast Asia add to the complexity and affect air quality in the region. Firework  
162 emissions are an example of extreme and regular local emissions in Southeast Asia. Even while  
163 several studies exist in the neighboring regions of East Asia (e.g., China) and South Asia (e.g.,  
164 India), there currently is no in-depth analysis of the chemical, physical, and optical properties of  
165 firework emissions in a Southeast Asian megacity where fireworks are culturally significant  
166 (Dela Piedra, 2018). This study is additionally novel because it includes the following  
167 combination of data types to investigate fireworks: size-resolved measurements (ionic/elemental  
168 composition, morphology), vertically-resolved data from a High Spectral Resolution Lidar  
169 (HSRL),  $\text{PM}_{2.5}$ , and meteorology. This work reports these data during the 2019 New Year  
170 celebrations in Metro Manila, Philippines, one of the most populated cities, with 12.88 M  
171 population (PSA, 2015). We address the following questions in order: (i) what are the conditions  
172 of the atmosphere during the study period in relation to aerosols, and how are these affected by  
173 firework emissions; (ii) what are the concentrations, mass size distributions, and morphological  
174 characteristics of different elemental and ionic species specific to fireworks, and how do these

175 affect bulk aerosol hygroscopicity? The results of this work provide new data that can help  
176 address how past and on-going firework emissions impact health, visibility, regional air quality,  
177 and biogeochemical cycling of nutrients and contaminants in the Philippines, Southeast Asia,  
178 and, more broadly, for all other cities with major firework events. It also contributes to the  
179 growing body of firework research findings (Devara et al., 2015).

180

## 181 **2. Methods**

### 182 2.1 Hourly PM<sub>2.5</sub> Mass Concentration

183 Hourly PM<sub>2.5</sub> mass concentrations were obtained to assess the evolution of and the temporal  
184 characteristics of fine particulates due to fireworks and their relation to meteorology and aerosol  
185 optical properties. The hourly PM<sub>2.5</sub> mass concentrations were collected at the Manila  
186 Observatory, Quezon City, Philippines (14.64° N, 121.08° E, ~70 m. a. s. l.) (Fig. S1) with a beta  
187 attenuation monitor (DKK-TOA Corporation) as part of the East Asia Acid Deposition  
188 Monitoring Network (EANET) (Totsuka et al., 2005). The beta attenuation monitor collects  
189 PM<sub>2.5</sub> samples on a ribbon filter, which are irradiated with beta particles. The attenuation of the  
190 beta particles through the sample and the filter is exponentially proportional to the mass loading  
191 on the filter. These hourly data were then averaged over 48-hour periods coinciding with water-  
192 soluble aerosol composition measurements (Section 2.5) before, during, and after the firework  
193 event.

194

### 195 2.2 Meteorological Data

196 Rainfall, temperature, relative humidity, and wind data were collected at the Manila Observatory  
197 with a Davis Vantage Pro2 Plus weather station (~90 m. a. s. l) before, during, and after the  
198 firework period. Hourly precipitation accumulation and 10-min averaged temperature, relative  
199 humidity, and wind were used for the analysis.

200

### 201 2.3 Back Trajectories

202 Three-day back trajectories with six-hour resolution were generated using the National Oceanic  
203 and Atmospheric Administration's (NOAA) Hybrid Single-Particle Lagrangian Integrated  
204 Trajectory (HYSPLIT) model (Rolph et al., 2017; Stein et al., 2015) using the Global Data  
205 Assimilation System (GDAS) with a resolution of 1°, and vertical wind setting of "model vertical  
206 velocity". To ascertain the impact of fireworks on surface particulate concentrations, back  
207 trajectories were chosen to end at the beginning times of the sampling periods before, during,  
208 and after the firework event. Trajectories were computed for an end point being at the Manila  
209 Observatory at an altitude of 500 m because it represents the mixed layer as done in other works

210 examining surface air quality (Mora et al., 2017; Aldhaif et al., 2020; Crosbie et al., 2014;  
211 Schlosser et al., 2017).

212

## 213 2.4 Remote Sensing

214 Vertical profiles of aerosol backscatter cross-section measured with the University of Wisconsin  
215 High Spectral Resolution Lidar (HSRL) which was deployed at the Manila Observatory in  
216 support of CAMP<sup>2</sup>EX. The HSRL instrument transmitting laser (Table S1) operates at 532 nm  
217 with 250 mW average power and pulse repetition rate of 4 KHz. The HSRL technique measures  
218 and separates the returned signal into the molecular and aerosol backscatter by using a beam  
219 splitter and an iodine absorption cell filter. The separated molecular signal allows for optical  
220 depth and backscatter cross section measurements in contrast to a standard backscatter lidar that  
221 requires assumption related to the particulate lidar ratio (Razenkov, 2010). The HSRL also  
222 measures particulate depolarization ratio, an indicator of aerosol or cloud particle shape with low  
223 depolarization indicative of spherical particles while intermediate values (10%) indicate a mix of  
224 spherical and nonspherical particles (Burton et al., 2014; Reid et al., 2017). HSRL data were  
225 uploaded and processed at the University of Wisconsin-Madison Space Science and Engineering  
226 Center server for periods before, during, and after the fireworks.

227 To verify the height values based on the vertical profiles of aerosol backscatter, the “surface-  
228 attached aerosol layer” height is estimated using the maximum variance method more commonly  
229 used for daytime convective boundary layer detection (Hooper and Eloranta, 1986). The height  
230 detection method is limited by the complexity of the firework event case due, however, to  
231 pertinent rain signals. The “surface attached aerosol layer” is derived from a 15-min moving  
232 window average based on the 30-s values.

233

## 234 2.5 Aerosol Composition and Morphology Measurements

235 Size-speciated PM (cut-point diameters: 18, 10, 5.6, 3.2, 1.8, 1.0, 0.56, 0.32, 0.18, 0.10, and  
236 0.056  $\mu\text{m}$ ) was collected on Teflon substrates (PTFE membrane, 2  $\mu\text{m}$  pores, 46.2 mm diameter,  
237 Whatman) with two Micro-Orifice Uniform Deposition Impactor (MOUDI II 120R, MSP  
238 Corporation) (Marple et al., 2014) samplers from the third floor of the main building (~85 m. a.  
239 s. l) at the Manila Observatory. Sample collection for each of the three MOUDI sets lasted 48  
240 hours before (13:30 December 24, 2018 to 13:30 December 26, 2018), during (14:45 December  
241 31, 2018 to 14:45 January 2, 2019), and after (13:30 January 1, 2019 to 13:30 January 3, 2019)  
242 firework activities. Note all times refer to local time (UTC + 8 hours). Although there were no  
243 fireworks released from the sampling site, there was firework activity in the immediate vicinity  
244 (~ 500 m from the sampling in all directions and all throughout the city in general). Firework  
245 activity around the sampling site began around ~19:00 on 31 December 2018, peaked at 00:00 of  
246 1 January 2019, and dropped drastically after. Based on PM<sub>2.5</sub> data there was no evidence of  
247 sustained firework activity past midnight. MOUDI samples collected before (December 24 to 26)  
248 and after (January 1 to 3) the firework event (December 31 to January 2) were considered as

249 background samples. Although there is some firework activity that is expected in the evening of  
250 December 24 (before the firework event), this is minimal compared to that which is the focus of  
251 this study (Dela Piedra, 2018; Santos Flora et al., 2010; Roca et al., 2015). The samples were  
252 covered with aluminum foil, sealed, and stored in the freezer before being shipped to the  
253 University of Arizona for elemental and ionic analysis.

254 Each sample substrate was cut in half. One half of each sample was extracted in 8 mL Milli-Q  
255 water (18.2 M $\Omega$ cm), sonicated, and analyzed for ions (ion chromatography (IC): Thermo  
256 Scientific Dionex ICS-2100 system) and elements (triple quadrupole inductively coupled plasma  
257 mass spectrometer: ICP-QQQ; Agilent 8800 Series). The remaining substrate halves were stored.  
258 Sample ionic and elemental concentrations were corrected by subtracting concentrations from  
259 background control samples. More information about the sampling and analysis are detailed in  
260 recent work (Stahl et al., 2020b). Limits of detection of the forty-one reported species are  
261 summarized in Table S3. Potassium (K<sup>+</sup>) was reported based on ICP-QQQ measurements rather  
262 than IC due to possible contamination from the KOH eluent used in the latter instrument. Non-  
263 sea salt SO<sub>4</sub><sup>2-</sup> was calculated by subtracting 0.2517 \* Na<sup>+</sup> from the total SO<sub>4</sub><sup>2-</sup> concentration  
264 (Prospero et al., 2003).

265 High-resolution scanning electron microscopy (SEM) combined with energy dispersive X-ray  
266 analysis (EDX) was used for examining particle morphology and chemical composition on a  
267 portion of the substrates collected during the firework event. Analyses were performed with a  
268 Hitachi S-4800 high-resolution SEM and a Thermo Fisher Scientific Noran Six X-ray  
269 Microanalysis System in the Kuiper Imaging cores at the University of Arizona. Approximately  
270 1 cm<sup>2</sup> was cut from the center of substrate halves and placed on double-sided carbon tape  
271 mounted on an aluminum stub. A thin layer (1.38 nm) of carbon was coated on the sample  
272 surface using a Leica EM ACE600 sputter coater to improve the sample's conductivity. SEM  
273 images were obtained at 15 keV and 30 keV acceleration voltages and with a 20  $\mu$ A probe  
274 current in high-magnification mode. The percentage contributions and the spatial distribution of  
275 the elements were obtained from the EDX analysis. Carbon, F, and Al should be ignored in the  
276 discussion of SEM-EDX results since C and F are present in the Teflon substrates, and the  
277 sample stub is an Al-rich substrate.

278 A total of 41 water-soluble species were detected in the 48-hr size-differentiated particulate  
279 samples collected before, during, and after the firework event. The total bulk mass concentration  
280 is defined as the sum of the concentrations of all the measured species across the MOUDI's  
281 eleven stages ( $\geq 0.056 \mu\text{m}$ ).

## 282 283 2.6 Enrichment Factor Calculations

284 To identify which species are most enhanced during fireworks, enrichment values are typically  
285 calculated using speciated concentrations during the fireworks relative to baseline periods  
286 (Tanda et al., 2019). We calculate water-soluble mass enrichment factors for each of the forty-  
287 one measured species by dividing their total bulk ( $\geq 0.056 \mu\text{m}$ ) mass concentrations during the  
288 firework event by the average of the total mass concentration of the species measured before and



289 after the firework event. Size-resolved enrichments were similarly calculated using measured  
290 mass concentrations for individual MOUDI stages. In a case when the mass concentration of a  
291 species during the firework event was non-zero but the mass concentrations during and after  
292 were zero (e.g., succinate), half of the detection limit was used in place of zero values.

293

## 294 2.7 Hygroscopicity Calculations

295 Hygroscopicity was calculated for particles ranging in size between 0.056 – 3.2  $\mu\text{m}$  before,  
296 during, and after the firework event. This size range was chosen to most closely be aligned with  
297 separate measurements of  $\text{PM}_{2.5}$  in the study (Section 2.1) that were used to account for the  
298 remaining mass not speciated in this study. We specifically calculate values for the single  
299 hygroscopicity parameter kappa,  $\kappa$  (Petters and Kreidenweis, 2007).

300 The water-soluble compound mass concentrations before, during, and after the firework event  
301 were calculated using an ion-pairing scheme (Gysel et al., 2007) for each MOUDI stage between  
302 diameters of 0.056 and 3.2  $\mu\text{m}$ , and then summed to achieve a total mass concentration for each  
303 compound in this size range. Black carbon mass concentrations in  $\text{PM}_{2.5}$  before and after the  
304 firework event were calculated based on their long-term (2001-2007) average contribution (32%)  
305 to  $\text{PM}_{2.5}$  mass in December and January (Cohen et al., 2009). Black carbon or elemental carbon  
306 (EC) concentrations during the firework event were assumed to be the average of the black  
307 carbon concentrations before and after the firework event. This was done because black carbon  
308 concentrations have been observed to not increase (Santos et al., 2007) as much as organic  
309 carbon (OC) (Lin, 2016), such that OC:EC mass ratios during fireworks have been observed to  
310 increase. Total non-water-soluble content between 0.056 and 3.2  $\mu\text{m}$  was calculated as the  
311 difference between the total  $\text{PM}_{2.5}$  mass concentration and the sum of the water-soluble species  
312 and black carbon mass concentrations. The mass of each species was divided by its density, and  
313 each of these volumes were added to quantify the volume of the measured aerosol (water-soluble  
314 compounds, black carbon, and organic matter) between 0.056 and 3.2  $\mu\text{m}$ . Volume fractions  
315 were then computed for each species. The Zdanovskii, Stokes, and Robinson (ZSR) mixing rule  
316 (Stokes and Robinson, 1966) was used to obtain the total hygroscopicity (total  $\kappa$ ) of the mixed  
317 aerosols by weighting  $\kappa$  values for the individual non-interacting compounds by their respective  
318 volume fractions and summing linearly. Densities and  $\kappa$  values for the individual compounds are  
319 based on those used elsewhere (AzadiAghdam et al., 2019), repeated in Table S4.

320

## 321 3. Results and Discussion

### 322 3.1 Hourly $\text{PM}_{2.5}$ , Meteorological, and Transport Patterns

323 We begin with hourly  $\text{PM}_{2.5}$  mass concentration results for the study period to provide context  
324 for the spatio-temporal characteristics of fine particulates due to fireworks, their interaction with  
325 meteorology, and effects on aerosol optical properties. Hourly  $\text{PM}_{2.5}$  (Fig. 1) began to increase  
326 from 44.0  $\mu\text{g m}^{-3}$  (shortly after rising above the 24-h Philippine National Ambient Air Quality

327 Guideline Value (NAAQGV) of  $50.0 \mu\text{g m}^{-3}$ ) after 18:00 time on 31 December 2018 with the  
328 beginning of firework activity and calm meteorological conditions. There was moderate (3 mm)  
329 rainfall from 22:00 to 23:00 that night as the firework activity began to increase. Rain is a sink  
330 for particles (Perry, 1999) and could have washed out some of the particulates in the air, thus  
331 potentially causing a slight dip in the hourly  $\text{PM}_{2.5}$  around midnight.  $\text{PM}_{2.5}$  peaked at  $383.9 \mu\text{g m}^{-3}$   
332 between 01:00 to 02:00 on 1 January 2019. The  $\text{PM}_{2.5}$  peak was delayed by approximately an  
333 hour from the peak firework activity at midnight possibly due to rainfall, relative humidity, and  
334 wind (Vecchi et al., 2008), in addition to aerosol dynamical processes requiring time for  
335 secondary aerosol formation and growth (Li et al., 2017). Minimal rain (0.2 mm in an hour) with  
336 high relative humidity (between  $93\% \pm 4\%$  to  $94\% \pm 4\%$ ) were conducive to aerosol growth  
337 and/or secondary particle formation. High relative humidity is related to aqueous-phase oxidation  
338 of  $\text{SO}_2$  (Sun et al., 2013) and  $\text{NO}_2$  (Cheng et al., 2014) as well as metal-catalyzed heterogeneous  
339 reactions (Wang et al., 2007) to form  $\text{SO}_4^{2-}$ . Aqueous oxidation has been found to be a  
340 predominant mechanism for the secondary formation of  $\text{SO}_4^{2-}$  during fireworks (Li et al., 2017),  
341 in addition to promoting secondary organic aerosol formation (Wonaschuetz et al., 2012; Youn  
342 et al., 2013). Light wind ( $\sim 1 \text{ m s}^{-1}$ ) after midnight from the northeast could also have transported  
343 more emissions from the populated Marikina Valley, located in the northeast, to the Manila  
344 Observatory contributing to the delay of the  $\text{PM}_{2.5}$  peak.

345 Particulate levels were enhanced for approximately 14 h from the beginning of the firework  
346 activity (Fig. 1) during which the average  $\text{PM}_{2.5}$  ( $143.4 \mu\text{g m}^{-3}$ ) exceeded the 24 h Philippine  
347 NAAQGV between 18:00 on 31 December 2018 to 08:00 on 1 January 2019. After 02:00 on 1  
348 January 2019,  $\text{PM}_{2.5}$  dropped quickly to  $122.0 \mu\text{g m}^{-3}$  between 03:00 to 04:00 (Fig. 1). The  $\text{PM}_{2.5}$   
349 decrease was less pronounced after 04:00 but continued decreasing steadily along with slight rain  
350 (0.4 mm in an hour) and light breeze ( $1 - 2 \text{ m s}^{-1}$ ) from the northwest to southwest directions.  
351 Firework activity in other countries have been documented to last from 2 – 6 h in a day and  
352 elevated particulate levels can be maintained for up to 6 – 18 h (Thakur et al., 2010; Crespo et  
353 al., 2012; Chatterjee et al., 2013; Kong et al., 2015; Tsai et al., 2012). The 48-h average  $\text{PM}_{2.5}$   
354 during ( $49.9 \mu\text{g m}^{-3}$ ) the firework event was 1.9 and 3.3 times more, respectively, than before  
355 ( $25.8 \mu\text{g m}^{-3}$ ) (Fig. S2) and after ( $15.2 \mu\text{g m}^{-3}$ ) (Fig. S3) the firework event. Two to three-fold  
356 increases in PM mass concentration due to fireworks have also been observed in other countries  
357 (Rao et al., 2012; Ravindra et al., 2003; Tsai et al., 2011; Shen et al., 2009). Greater increases ( $>$   
358 5 times) in particulate mass concentrations elsewhere were related to more intense and prolonged  
359 (lasting several days) firework activity (Tian et al., 2014).

360 Three-day back trajectories for the period before the firework event were from the northeast to  
361 east directions coming from the Philippine Sea (Fig. 2a). For the periods (Fig. 2b) during and  
362 (Fig. 2c) after the firework event, back trajectories were from the northeast to east/northeast  
363 directions. The general wind directions from the back trajectories are consistent with the  
364 climatologically prevailing northeasterly monsoonal winds in December and January for the  
365 Philippines (Villafuerte II et al., 2014). The origin of the air parcels did not have any major  
366 emissions events that could have impacted the measurements after long-range transport. This is

367 important to note because the tracers for fireworks are also tracers for transported emissions due  
368 to biomass burning ( $K^+$ ) (Braun et al., 2020) and industrial activities (Cohen et al., 2009). Thus,  
369 enriched particulate concentrations during the firework activity were most likely locally  
370 produced. One factor impacting surface PM concentrations is the vertical structure of the lower  
371 troposphere, which is addressed in the next section based on HSRL data.

372

### 373 3.2 Optical Aerosol Properties

374 Heavy aerosol loading at the surface was observed up to eight hours after the fireworks peak  
375 (00:00) with high HSRL 532 nm backscatter cross-section and depolarization (Fig. 3a) reaching  
376 ~440 m above the ground. Prior to the firework peak, the surface aerosol layer had lower  
377 backscatter (before 22:00, Fig. 3a), and this cleaner condition is shown by the 16:16 local time  
378 vertical profile of the aerosol backscatter (Fig. 3b). Rainfall (Fig. 1a) contributed to columns of  
379 high backscatter (Fig. 3a) after 22:00 and before the firework peak with a measurable decrease in  
380 the aerosol backscatter for a short time after the precipitation (23:00 and 00:00).

381 As confirmed by height detection, aerosols reached up to ~440 m (Fig 3a and b) at 00:00 (1  
382 January 2019). It persisted for at least an hour then dropped to  $118 \pm 20$  m with higher aerosol  
383 backscatter retained until January 1, 2019 08:00. Some of the smoke is above the detected height  
384 (i.e. 01:00).

385

### 386 3.3 Mass Size Distributions

387 Building on the previous results describing the general environmental conditions during the  
388 study period, now we focus on the detailed size-resolved measurements. The total water-soluble  
389 bulk mass concentration (Table 1) during the firework event ( $16.74 \mu\text{g m}^{-3}$ ) was 5.71 times and  
390 4.73 times higher than the total bulk mass concentrations before ( $2.93 \mu\text{g m}^{-3}$ ) and after ( $3.54 \mu\text{g}$   
391  $\text{m}^{-3}$ ) the firework event, respectively. Assuming the average of the water-soluble mass  
392 concentrations before and after the firework event represent background values, this translates to  
393 an 80.66% increase in water-soluble mass during the firework event.

394 The firework event was associated with increased total water-soluble mass fraction (32.33%)  
395 ( $0.056 - 3.2 \mu\text{m}$  size range, Section 3.1) in  $\text{PM}_{2.5}$  (Fig. S4) compared to before (9.90%) and after  
396 (17.79%) the firework event. The water-soluble particulate mass fraction in  $\text{PM}_{2.5}$  similarly  
397 increased in other firework events (Yang et al., 2014). The highest total water-soluble mass  
398 concentrations during the firework event were from the following ions: non-sea salt (nss)  $\text{SO}_4^{2-}$   
399 ( $6.81 \mu\text{g m}^{-3}$ ),  $K^+$  ( $5.05 \mu\text{g m}^{-3}$ ),  $\text{NO}_3^-$  ( $1.70 \mu\text{g m}^{-3}$ ),  $\text{Cl}^-$  ( $1.46 \mu\text{g m}^{-3}$ ),  $\text{Mg}^{2+}$  ( $0.37 \mu\text{g m}^{-3}$ ),  $\text{Na}^+$   
400 ( $0.33 \mu\text{g m}^{-3}$ ), and  $\text{Ca}^{2+}$  ( $0.30 \mu\text{g m}^{-3}$ ). These contributed to 95.75% of the total detected bulk  
401 water-soluble mass concentration then.

402 Total water-soluble bulk mass concentration during the firework event was dominated by  
403 submicrometer particles, which accounted for 77.4% of the total water-soluble bulk mass (Fig.  
404 4b). Supermicrometer mass fractions were greater before (Fig. 4a) and after (Fig. 4c) the  
405 firework event (43.7% and 57.5% of the water-soluble bulk mass concentration) compared to  
406 during the firework event (22.6%). The increase in submicrometer mass fractions is typical with  
407 firework emissions (Crespo et al., 2012; Do et al., 2012). In New York, fireworks contributed to  
408 77% of PM<sub>1</sub> due to potassium salts and oxidized organic aerosol (Zhang et al., 2019).

409 Non-sea salt SO<sub>4</sub><sup>2-</sup> had the highest contribution (40.7%) to total water-soluble bulk mass  
410 concentration during the firework event (Table 1). Sulfate exhibited a shift in its mass size  
411 distribution to a slightly larger size during firework activity (Fig. 4b). During the firework event,  
412 87.13 % of the nss-SO<sub>4</sub><sup>2-</sup> was in the 0.32 μm to 1.8 μm size fraction. Before and after the  
413 firework event, 87.28% and 85.14% of the nss-SO<sub>4</sub><sup>2-</sup> mass concentration, respectively, was  
414 distributed in a finer size fraction (0.18 μm to 1 μm) (Fig. 4a and 4c).

415 Potassium contributed 30.19% to the total water-soluble mass concentration during the firework  
416 event (Table 1), presumably in the form of KNO<sub>3</sub>. This compound is associated with black  
417 powder used as a propellant (Li et al., 2017). Potassium's mass concentration distribution  
418 similarly shifted to a slightly larger size during the firework event (Figure 4b). Most (87.6%) of  
419 the bulk K<sup>+</sup> mass concentration during the firework event was between 0.32 and 1.8 μm,  
420 compared to 85.4% and 79.4% between 0.18 and 1 μm before and after the firework event,  
421 respectively (Fig. 4a and 4c).

422 The shift in the mass size distribution of K<sup>+</sup> and nss-SO<sub>4</sub><sup>2-</sup> can be due to the removal of  
423 nucleation-mode particles as a result of increased coagulation in the accumulation mode (Zhang  
424 et al., 2010). Relatively larger SO<sub>4</sub><sup>2-</sup> particles can also be due to secondary sources rather than  
425 primary sources, and aging could have also contributed to particle growth as has been suggested  
426 for firework particles in Nanning, China (Li et al., 2017). Firework emissions include gases like  
427 SO<sub>2</sub> which undergo aqueous uptake and oxidation onto particles to form SO<sub>4</sub><sup>2-</sup>. Furthermore,  
428 enhanced secondary formation is aided by metals emitted during fireworks that help convert SO<sub>2</sub>  
429 to SO<sub>4</sub><sup>2-</sup> (Feng et al., 2012; Wang et al., 2007).

430 Nitrate, Cl<sup>-</sup>, and Mg<sup>2+</sup> mass size distributions all exhibited pronounced peaks in the  
431 submicrometer range during the firework event (Fig. 5). The mass sum concentration of the  
432 aforementioned ions peaked (46.39% of the total mass concentration of the three species)  
433 between 0.56 and 1.0 μm. On the other hand, their mode appeared between 1.8 and 3.2 μm  
434 before and after the firework event (33.02% and 32.91% of the total mass concentration of the  
435 three species, respectively) (Fig. 5). Nitrate, Cl<sup>-</sup>, and Mg<sup>2+</sup> are emitted during fireworks (Zhang et  
436 al., 2017) as finer-sized submicrometer particles (Tsai et al., 2011) compared to background  
437 conditions when these species are mostly associated with coarser supermicrometer particles  
438 (AzadiAghdam et al., 2019; Cruz et al., 2019; Hilario et al., 2020). Nitrate can also be formed  
439 secondarily (Yang et al., 2014) from firework emissions. Firework emissions are associated with  
440 lower NO<sub>3</sub><sup>-</sup>:SO<sub>4</sub><sup>2-</sup> ratios (Feng et al., 2012) compared to days dominated by mobile sources

441 (Arimoto et al., 1996) due to different formation mechanisms (Tian et al., 2014). Consistent with  
442 the literature, low  $\text{NO}_3^-:\text{SO}_4^{2-}$  ratios were also observed during the firework event (before: 0.79,  
443 during: 0.25, after: 0.82). A low  $\text{NO}_3^-:\text{SO}_4^{2-}$  ratio is related to decreased pH of the particles (Cao  
444 et al., 2020), which may impact not just air quality and health but also nearby waterbodies where  
445 the particles may deposit. It is important to note that background supermicrometer  $\text{Cl}^-$  and  $\text{Mg}^{2+}$   
446 in Manila are most likely associated with sea salt while background supermicrometer  $\text{NO}_3^-$   
447 possibly in the form of  $\text{NaNO}_3$  (de Leeuw et al., 2001) or  $\text{NH}_4\text{NO}_3$  likely stems from partitioning  
448 of nitric acid gas onto surfaces (de Leeuw et al., 2001) of coarse particles such as sea salt and  
449 dust (AzadiAghdam et al., 2019; Cruz et al., 2019). The  $\text{Cl}^-:\text{Na}^+$  mass ratio during the firework  
450 event increased to 4.44 (from 0.69 and 1.08 before and after, respectively) and was higher than  
451 the typical  $\text{Cl}^-:\text{Na}^+$  ratio in seawater of 1.81 (Braun et al., 2017). These ratio results confirm that  
452 the increase in  $\text{Cl}^-$  concentrations during the firework event is not driven by sea salt but instead  
453 linked to firework emissions. The lack of increased sea salt influence during the firework event,  
454 which is not to be expected, is further confirmed by relatively small changes in the amount of  
455 observed  $\text{Na}^+$ , as will be discussed subsequently.

456 The  $\text{Na}^+$ ,  $\text{Ca}^{2+}$ , and  $\text{NH}_4^+$  mass size distributions peak in the supermicrometer range (1.8 to 3.2  
457  $\mu\text{m}$ ) (Figure S5) and total mass concentrations (Table 1) varied minimally, relative to the earlier  
458 mentioned species, before ( $0.33 \mu\text{g m}^{-3}$ ,  $0.21 \mu\text{g m}^{-3}$ ,  $0.21 \mu\text{g m}^{-3}$ , respectively), during ( $0.33 \mu\text{g}$   
459  $\text{m}^{-3}$ ,  $0.30 \mu\text{g m}^{-3}$ ,  $0.19 \mu\text{g m}^{-3}$ ) and after ( $0.53 \mu\text{g m}^{-3}$ ,  $0.38 \mu\text{g m}^{-3}$ ,  $0.28 \mu\text{g m}^{-3}$ ) the firework  
460 event. The minimal change in  $\text{NH}_4^+$  mass concentration is most likely due to little or no variation  
461 of its precursor gas (e.g.,  $\text{NH}_3$ ) due to firework activities and the fact that firework materials are  
462 commonly composed of K-rich salts rather than  $\text{NH}_4^+$  salts (Zhang et al., 2019). The latter seems  
463 probable because the K:S mass ratios of 2.75 and 2.71, observed from 0.18 – 0.32  $\mu\text{m}$  and 0.32 –  
464 0.56  $\mu\text{m}$ , respectively, during the firework event suggests a firework-related source of K and S.  
465 This ratio is similar to the K:S ratio of 2.75 (Dutcher et al., 1999) of “black powder” (Perry,  
466 1999), a type of pyrotechnic comprised of K and S.

467 The mass size distribution for the sum of the rest of the species (“others” in Fig. 4) shifted from  
468 having a peak at the smaller end of the accumulation mode (0.18 – 0.32  $\mu\text{m}$ ) before and after the  
469 firework event to larger sizes in the accumulation mode (0.56 – 1.0  $\mu\text{m}$ ) during the firework  
470 event. The shift in mode to slightly larger particles during the firework event may be due to  
471 increased coagulation sinks (Zhang et al., 2010) and secondary production (Retama et al., 2019).  
472 An additional coarse peak (3.2 – 5.6  $\mu\text{m}$ ) observed after the firework event is mainly attributed  
473 to sea salt constituents (e.g.,  $\text{Cl}^-$ ,  $\text{Na}^+$ ) and likely unrelated to firework emissions aging and  
474 processing. The mass contribution of the “others” to the total measured water-soluble mass  
475 concentration decreased during the firework event to 4.3% from 12.5% before and 11.6% after  
476 the firework event due to the prevalence of the ionic species ( $\text{nss-SO}_4^{2-}$ ,  $\text{K}^+$ ,  $\text{NO}_3^-$ ,  $\text{Cl}^-$ ,  $\text{Mg}^{2+}$ ,  $\text{Na}^+$ ,  
477  $\text{Ca}^{2+}$ , and  $\text{NH}_4^+$ ) discussed earlier (Table 1).

478

479 3.4 Enriched Tracers in Firework Emissions

480 Here we more closely examine how much concentrations of species changed during the firework  
481 event. Bulk mass concentrations of eighteen of the forty-one measured species were enriched  
482 during the firework event by more than two times compared to the average of their bulk mass  
483 concentrations before and after the firework event (Fig. 5). Enrichments for Cu (65.2), Sr (24.4),  
484 succinate (19.4), Ba (18.2),  $K^+$  (16.3),  $nss-SO_4^{2-}$  (9.8), Al (6.9), Pb (6.1), and maleate (5.3) were  
485 highest ( $> 5$ ) among the species measured (Fig.5). Potassium and  $nss-SO_4^{2-}$  together contributed  
486 to 70.9% of the total measured species during the firework event (Table 1). However, Cu, Sr,  
487 succinate, Ba, Al, Pb, and maleate contributed a total of only 2.1% to the total measured species  
488 mass concentration. This reinforces the importance of looking at enrichments rather than  
489 absolute mass concentrations for identifying which aerosol constituents are firework tracers.  
490 Tracer metals in firework emissions were previously shown to contribute a small fraction  
491 ( $\sim < 2\%$ ) to total PM mass (Jiang et al., 2014).

492 Of the eighteen species with observed enrichments exceeding two (Fig. 5), only those which are  
493 firework components and that are uninfluenced by secondary formation are considered tracers.  
494 The identified fourteen firework tracers based on these criteria are as follows: Cu, Sr, Ba,  $K^+$ , Al,  
495 Pb,  $Mg^{2+}$ , Cr, Tl,  $Cl^-$ , Mn, Rb, Zn, and Ag. Metals are usually in the form of  $Cl^-$  salts in fireworks  
496 (Wang et al., 2007). In this study, the enrichment of  $Cl^-$  during the firework event was found to  
497 be 3.7. Some of the identified tracer metals are regulated and their detection is of concern.  
498 Magnesium is not recommended as a firework component because it is sensitive to heat and can  
499 easily ignite in storage (Do et al., 2012). Lead is highly toxic and thus regulated (Moreno et al.,  
500 2010) as its occurrence in fireworks is a serious health hazard. Although  $SO_4^{2-}$ , maleate (fuel),  
501 and  $NO_3^-$  (oxidant) were also enriched more than two times during the firework event and are  
502 also firework components (Zhang et al., 2019), they can be formed secondarily via gas-to-  
503 particle conversion processes (Yang et al., 2014) and are not considered as firework tracers.  
504 Succinate is likewise formed secondarily and is not considered a firework tracer (Wang et al.,  
505 2007). The identified firework tracers with the highest enrichments ( $> 5$ ) (excluding  $K^+$ ),  
506 including Cu, Sr, Ba, Al, and Pb, together contributed 2.1% to the total measured species mass  
507 concentration during the firework event (Table 1).

508 Size-resolved enrichments (Fig. 6) were highest in the submicrometer range for most measured  
509 species. This is consistent with past studies such as in Italy (Vecchi et al., 2008), Taiwan (Do et  
510 al., 2012), and Spain (Crespo et al., 2012) where elemental concentrations due to pyrotechnics  
511 increased in the submicrometer mode. The peak size differentiated enrichments of the first five  
512 firework tracers Sr (45.08), Ba (57.82),  $K^+$  (48.70), Al (18.75), and Pb (69.07) were in the 1.0 –  
513 1.8  $\mu m$  size range. Copper (49.85) peaked between 0.56 – 1.0  $\mu m$  because it did not have valid  
514 data for diameters exceeding 1.0  $\mu m$ . Strontium and Ba had very high enrichments (254.40 and  
515 195.84) from 0.1 – 0.18  $\mu m$  due to very low concentrations before and after the firework event in  
516 that size range. Enrichments of up to  $\sim 1000$  (Crespo et al., 2012) for Sr and Ba have been  
517 observed due to pyrotechnics, and both are known firework tracers (Kong et al., 2015).

518 The size-resolved enrichments of other notable species (Fig. 6 and Fig. S6) peaked at specific  
519 size ranges between 0.32 – 1.8  $\mu m$ :  $Mg^{2+}$  (18.93, 0.056 – 0.1  $\mu m$ ), Cr (14.37, 1.0 – 1.8  $\mu m$ ), Tl

520 (18.12, 0.56 – 1.0  $\mu\text{m}$ ),  $\text{Cl}^-$  (170.94, 0.32 – 0.56  $\mu\text{m}$ ), Mn (6.29, 1.0 – 1.8  $\mu\text{m}$ ), Rb (6.87, 1.0 –  
521 1.8  $\mu\text{m}$ ),  $\text{NO}_3^-$  (7.26, 0.56 – 1.0  $\mu\text{m}$ ), Cs (6.28, 1.0 – 1.8  $\mu\text{m}$ ), Mo (4.15, 0.32 – 0.56  $\mu\text{m}$ ), Ti  
522 (6.63, 0.32 – 0.56  $\mu\text{m}$ ), Co (17.94, 0.56 – 1.0  $\mu\text{m}$ ), and methanesulfonate (MSA) (6.66, 0.56 –  
523 1.0  $\mu\text{m}$ ). Among all the measured water-soluble species,  $\text{Cl}^-$  had the highest size-resolved  
524 enrichment, followed by Sr, Ba,  $\text{K}^+$ , Pb, and Cu. This is expected because inorganic salts  
525 comprise an enormous percentage of firework emissions (Martín-Alberca et al., 2016).

526

### 527 3.5 SEM-EDX

528 In addition to size-resolved species concentrations, the morphology of particles is important with  
529 regard to their optical properties, hygroscopicity, and their transport behavior. Five SEM  
530 images from the different stages (0.18 – 1  $\mu\text{m}$ ) of the MOUDI sampler with possible firework  
531 influence are highlighted (Fig. 7). There were signs of nano-scale aggregation that were chain-  
532 like and reminiscent of soot particles from pyrolysis and combustion (Pirker et al., 2020; Pósfai  
533 et al., 2003; D’Anna, 2015) in all of the images, and especially distinct in the 0.1 – 0.18  $\mu\text{m}$  (Fig.  
534 4b) and 0.18 – 0.32  $\mu\text{m}$  (Fig.7c) stages. Images for larger sizes revealed relatively larger particles  
535 appearing as a translucent crystal-shaped rectangle in the 0.32 – 0.56  $\mu\text{m}$  image (Fig. 7d), in  
536 addition to a capsule-shaped particle (Fig. 7e) and a cubic-shaped particle (Fig. 7f) in the two  
537 0.56 – 1.0  $\mu\text{m}$  images. The presence of such non-spherical shapes including chain aggregates  
538 points to the potential for particle collapse and shrinking associated with humidified conditions  
539 as noted in past work (Shingler et al., 2016 and references therein).

540 The chemical composition of the blank Teflon substrate (Fig. 7a) was examined first by EDX to  
541 determine the background signals before the actual samples were analyzed. The color intensity of  
542 the element maps (Fig. S7) relates the concentration of the analyzed element relative to the  
543 backscattered electron image (gray-scale) of the sample. The background substrate was  
544 dominated by C, F, and Al (bright yellow, bright blue, and bright blue-green, respectively, in Fig.  
545 S7-a1/a2/a3). Metallic elements were distributed in each of the five featured SEM images.  
546 Molybdenum and K were present in all of the substrate stages (bright red in Fig. S7-  
547 b3/b4/c3/c8/d7/d8/e6/e7/f6/f9). Other metals were also found in the different stages such as K,  
548 Mg, Al, Ru, Pd, Ba, Hf, and Tl. The identified heavy metals in the particles are commonly used  
549 in firework as fuel components, colorants, and oxidants (Singh et al., 2019). Potassium, Mg, Al,  
550 Ba, and Tl are in the group of firework tracers that were already identified (Section 3.4 and Fig.  
551 5) to have mass bulk concentration enrichments exceeding two. Molybdenum exhibited a  
552 reduced mass bulk concentration enrichment of 1.93 (Fig. 5), but had size-resolved enrichments  
553 between 1.21 and 4.15 (Fig. 6) in the substrate cut-outs analyzed for EDX. The cube-shaped  
554 feature in the 0.56 – 1.0  $\mu\text{m}$  substrate appears to be KCl because of the high color density of K  
555 and Cl in the elemental maps (bright red and bright blue-green in Fig. S7-f6/f8) and because the  
556 shape of KCl is cubic (Pirker et al., 2020). The crystal-shaped rectangle in the 0.32 – 0.56  $\mu\text{m}$   
557 range appears to be enriched by Cl (bright blue-green in Fig. S7-d6). The same applies to the  
558 capsule-shaped particle in 0.56 – 1.0  $\mu\text{m}$  image (bright blue-green in Fig. S7-e5). The chloride

559 ion ( $\text{Cl}^-$ ) is a component of metal salts, usually in the form of  $\text{ClO}_4^-$  or  $\text{ClO}_3^-$  (Tian et al., 2014)  
560 used to color fireworks (Shimizu, 1988).

561 These results of the sampled portions of the substrate stages are consistent with the results of the  
562 size-resolved submicrometer enrichments measured by IC and ICP-QQQ (Section 3.4) for Mo,  
563 K, Mg, Al, Ba, and Tl. Molybdenum was brightest red in the 0.32 – 0.56  $\mu\text{m}$  image (Fig. S7-d8),  
564 consistent with the highest enrichments (4.15 in Fig. 6) for that size range. Potassium was  
565 brightest red in the 0.56 – 1.0  $\mu\text{m}$  image (Fig. S7-e6/f6), consistent with highest enrichments  
566 (33.04 in Fig. 6). Magnesium was brightest yellow from 0.32 – 1.0  $\mu\text{m}$  (Fig. S7-d4/e3/f4),  
567 consistent with highest enrichments (9.50 and 11.58 in Fig. 6). Aluminum had a high signal in  
568 the blank Teflon substrate but also was brightest blue-green (Fig. S7-d5/e4/f5) in between 0.32 –  
569 1.0  $\mu\text{m}$  in the sample during the firework event, consistent with highest enrichments (9.22 and  
570 13.32 in Fig. 6). Barium was detected by EDX between 0.56 – 1.0  $\mu\text{m}$  (Fig. S7-f11 where its  
571 enrichment was 12.39 (Fig. 6). Thallium was detected between 0.56 and 1.0  $\mu\text{m}$  (Fig. S7-f13) by  
572 EDX, where its enrichment was highest (18.12 in Fig. 7) as detected by ICP-QQQ. The  
573 submicrometer metal salts due to fireworks can uptake water at high humidity (ten Brink et al.,  
574 2018).

575

### 576 3.6 Hygroscopicity Analysis

577 As fireworks alter the chemical profile of ambient PM, we estimate how aerosol hygroscopicity  
578 responded during fireworks relative to periods before and after. For reference, typical  $\kappa$  values  
579 range from 0.1 to 0.5 for diverse air mass types such as urban, marine, biogenic, biomass  
580 burning, and free troposphere (Dusek et al., 2010; Hersey et al., 2013; Shingler et al., 2016;  
581 Shinzuka et al., 2009). AzadiAghdam et al. (2019) reported size-resolved values ranging from  
582 0.02 to 0.31 using data from the same field site in Metro Manila but for a different time period  
583 and without any firework influence (July – December 2018). They found the highest values to be  
584 coincident with MOUDI stages with most sea salt influence (3.2 – 5.6  $\mu\text{m}$ ).

585 For this study, a bulk  $\kappa$  value is reported for the size range between 0.056 – 3.2  $\mu\text{m}$  as noted in  
586 Section 2.7, and subsequent references to composition data are for this size range. Kappa was  
587 enhanced during the firework event (0.18) compared to before (0.11), due mostly to increased  
588 contributions from  $\text{K}_2\text{SO}_4$  and  $\text{Mg}(\text{NO}_3)_2$  (Fig. 8a). This is expected because based on the ZSR  
589 mixing rule (Stokes and Robinson, 1966) the bulk hygroscopicity ( $\kappa$ ) is dependent on the sum of  
590 the  $\kappa$  values for individual non-interacting compounds weighted by their respective volume  
591 fractions. More specifically, the volume fractions of  $\text{K}_2\text{SO}_4$  and  $\text{Mg}(\text{NO}_3)_2$  increased from 0.01  
592 to 0.10 and 0.01 to 0.03, respectively (Fig. 8b). Notable reductions in volume fraction during the  
593 firework event were for  $\text{NaNO}_3$  (0.01 to 0.00), black carbon (0.26 to 0.12), and  $(\text{NH}_4)_2\text{SO}_4$  (0.02  
594 to 0.01) (Fig. 8b). All three species are not associated with primary firework emissions. Although  
595  $\text{NaNO}_3$  and  $(\text{NH}_4)_2\text{SO}_4$  are hygroscopic, their decreased volume fractions happened alongside a  
596 decreased volume fraction of non-hygroscopic black carbon and increased volume fractions of



597 the firework-related and hygroscopic  $K_2SO_4$  and  $Mg(NO_3)_2$ , which increased bulk aerosol  
598 hygroscopicity during the firework event.

599 Kappa decreased to an intermediate value after the firework event (0.15) (Fig. 8a); this value  
600 exceeds that from before the fireworks owing partly to more sea salt influence that was unrelated  
601 to fireworks. The change in volume fraction of sea salt from before and during fireworks (0.01)  
602 to after the fireworks (0.03) (Fig. 8b) translated to an increase of 0.03 in bulk  $\kappa$  (Fig. 8a) from  
603 before to after the firework event. Although fireworks emit extensive amounts of inorganic  
604 species, the calculated  $\kappa$  values were still relatively low because the background air is dominated  
605 by organics and black carbon, which are relatively hydrophobic species (Table S4) (Cohen et al.,  
606 2009; Oanh et al., 2006; Cruz et al., 2019).

607

#### 608 **4. Conclusion**

609 This study reports on important aerosol characteristics measured during the 2019 New Year  
610 fireworks in Metro Manila. Notable results of this work, following the order of questions raised  
611 at the end of Section 1, are as follows:

- 612 • Firework activities caused significant enhancement of  $PM_{2.5}$  reaching a maximum of  
613  $383.9 \mu g m^{-3}$  between 01:00 to 02:00 on 1 January 2019. Surface aerosol loading  
614 increased over a period of eight hours during the firework event, coincident with peak  
615  $PM_{2.5}$  levels. The heaviest aerosol layer measured by the HSRL lidar was observed for at  
616 least an hour, and reached  $\sim 440$  m above the surface, after which the aerosol layer  
617 dropped to  $118 \pm 20$  m. Aerosol backscatter during the firework activity decreased  
618 noticeably for short periods after rainfall. Besides rainfall, wind, and relative humidity  
619 also possibly contributed to washout, local dispersion, and secondary formation of  
620 particles, respectively. There was no significant influence from long-range transport to  
621 the sampling site, confirming that the sample data was most representative of the local  
622 nature of particulate enhancements observed during the firework event.
- 623 • The firework event enhanced bulk concentrations of water-soluble aerosol species,  
624 especially in the submicrometer range. Mass size distributions of the water-soluble  
625 species shifted to slightly larger accumulation-mode sizes most likely due to increased  
626 coagulation sinks and secondary formation. Potassium and  $nss-SO_4^{2-}$  were the major  
627 water-soluble contributors. Cubic and capsule-shaped  $Cl^-$ -rich particles were prominent in  
628 submicrometer particles collected during the firework event, suggesting the presence of  
629  $KCl$ . Inorganic species including  $Cu$ ,  $Sr$ ,  $Ba$ ,  $K^+$ ,  $Al$ ,  $Pb$ ,  $Mg^{2+}$ ,  $Cr$ ,  $Tl$ ,  $Cl^-$ ,  $Mn$ ,  $Rb$ ,  $Zn$ ,  
630 and  $Ag$  were enriched more than two times by mass during the firework event as  
631 compared to before and after the event. While the most enriched inorganic firework  
632 tracers, including  $Cu$ ,  $Sr$ ,  $Ba$ ,  $Al$ , and  $Pb$  (excluding  $K^+$ ), comprised only 2.1% of the total  
633 water-soluble mass, their contribution is significant because they support findings that the  
634 samples represent firework emissions. The increased volume fractions of inorganics

635 increased aerosol hygroscopicity ( $\kappa$ ) between 0.056 and 3.2  $\mu\text{m}$  from 0.11 (before the  
636 fireworks) to 0.18 during the firework event.

637 Fireworks caused unhealthy levels of  $\text{PM}_{2.5}$  that exceeded the Philippine ( $50.0 \mu\text{g m}^{-3}$ ), U.S.  
638 ( $35.0 \mu\text{g m}^{-3}$ ), and World Health Organization (WHO,  $25.0 \mu\text{g m}^{-3}$ ) standards for  $\text{PM}_{2.5}$  over 24  
639 hours. The brief but sharply enhanced concentrations of water-soluble species in the  
640 submicrometer size range, especially for  $\text{K}^+$  and  $\text{SO}_4^{2-}$ , have implications for both public health  
641 and the environment, the former of which is owing to how smaller particles can penetrate more  
642 deeply into the human respiratory system. Some of the components detected during the fireworks  
643 were submicrometer  $\text{Pb}$  and  $\text{Mg}^{2+}$ , which is of concern because these are banned substances due  
644 to their being health and fire hazards, respectively. The presence of  $\text{Pb}$  in the firework emissions  
645 exacerbates the presence of submicrometer  $\text{Pb}$  in Metro Manila (Gonzalez et al., 2021). The  
646 results show the opportunity that improved quality and management of fireworks can have for  
647 better local air quality.

648 Higher concentrations of secondary particles in the accumulation mode from fireworks are  
649 related to increased mass extinction efficiency and therefore decreased visibility (Jiang et al.,  
650 2014), as was observed in this study. The increased water-soluble fraction, especially in the  
651 submicrometer mode, during firework events coincides with elevated particle hygroscopicity,  
652 which is related to CCN activity (Drewnick et al., 2006) at smaller diameters (Yuan et al., 2020),  
653 with implications that can be better assessed in a future study. The atmospheric environment in  
654 Southeast Asia, coupled with increasing emissions and extreme sources such as fireworks, offers  
655 a unique field laboratory for the study of aerosol aqueous processes.

656

## 657 **Data availability**

658 High Spectral Resolution Lidar data collected at Manila Observatory can be found at:  
659 (University of Wisconsin Lidar Group) [http://hsrl.ssec.wisc.edu/by\\_site/30/custom\\_rti/](http://hsrl.ssec.wisc.edu/by_site/30/custom_rti/)

660 Size-resolved aerosols data collected at Manila Observatory can be found at: (Stahl et al., 2020a)  
661 on figshare as well as on the NASA data repository at  
662 DOI:10.5067/Suborbital/CAMP2EX2018/DATA001.

663

## 664 **Author Contributions**

665 MTC, MOC, JBS, RAB, ABM, CS, and AS designed the experiments. All coauthors carried out  
666 various aspects of the data collection. MTC, EE, SV, RH, GL, LM, CS, and AS conducted  
667 analysis and interpretation of the data. EE, LM, SV, RH, GL, and AS prepared the manuscript  
668 with contributions from the coauthors.

669

670 **Competing Interests**

671 The authors declare that they have no conflict of interest.

672

673 **Acknowledgements**

674 The authors acknowledge support from NASA grant 80NSSC18K0148 in support of the NASA  
675 CAMP<sup>2</sup>Ex project. R. A. Braun acknowledges support from the ARCS Foundation. M. T. Cruz  
676 acknowledges support from the Philippine Department of Science and Technology's ASTHRD  
677 Program. A. B. MacDonald acknowledges support from the Mexican National Council for  
678 Science and Technology (CONACYT). We acknowledge Agilent Technologies for their support  
679 and Shane Snyder's laboratories for ICP-QQQ data. We thank the Department of Environment  
680 and Natural Resources Environmental Management Bureau (DENR-EMB) Central Office Air  
681 Quality Management Section in the Philippines and the Air Center for Air Pollution Research in  
682 Japan of EANET for the hourly PM<sub>2.5</sub> data. The tradition of sampling the New Year air quality in  
683 Metro Manila was instilled by Fr. Dan McNamara, SJ, Fr. Jett Villarin, SJ, and Gemma Narisma,  
684 and for this we are grateful.

685

686 **References**

687 Agus, E. L., Lingard, J. J., and Tomlin, A. S.: Suppression of nucleation mode particles by  
688 biomass burning in an urban environment: a case study, *Journal of Environmental Monitoring*,  
689 10, 979-988, 2008.

690 Aldhaif, A. M., Lopez, D. H., Dadashazar, H., and Sorooshian, A.: Sources, frequency, and  
691 chemical nature of dust events impacting the United States East Coast, *Atmospheric*  
692 *Environment*, 117456, 2020.

693 Alpert, D. J., and Hopke, P. K.: A determination of the sources of airborne particles collected  
694 during the regional air pollution study, *Atmospheric Environment* (1967), 15, 675-687, 1981.

695 Arimoto, R., Duce, R., Savoie, D., Prospero, J., Talbot, R., Cullen, J., Tomza, U., Lewis, N., and  
696 Ray, B.: Relationships among aerosol constituents from Asia and the North Pacific during PEM-  
697 West A, *Journal of Geophysical Research: Atmospheres*, 101, 2011-2023, 1996.

698 AzadiAghdam, M., Braun, R. A., Edwards, E.-L., Bañaga, P. A., Cruz, M. T., Betito, G.,  
699 Cambaliza, M. O., Dadashazar, H., Lorenzo, G. R., and Ma, L.: On the nature of sea salt aerosol  
700 at a coastal megacity: Insights from Manila, Philippines in Southeast Asia, *Atmospheric*  
701 *Environment*, 216, 116922, 2019.

702 Barman, S., Singh, R., Negi, M., and Bhargava, S.: Ambient air quality of Lucknow City (India)  
703 during use of fireworks on Diwali Festival, *Environmental monitoring and assessment*, 137, 495-  
704 504, 2008.

705 Becker, J. M., Iskandrian, S., and Conkling, J.: Fatal and near-fatal asthma in children exposed to  
706 fireworks, *Annals of Allergy, Asthma & Immunology*, 85, 512-513, 2000.

707 Beig, G., Chate, D., Ghude, S. D., Ali, K., Satpute, T., Sahu, S., Parkhi, N., and Trimbake, H.:  
708 Evaluating population exposure to environmental pollutants during Deepavali fireworks displays  
709 using air quality measurements of the SAFAR network, *Chemosphere*, 92, 116-124, 2013.

710 Braun, R. A., Dadashazar, H., MacDonald, A. B., Aldhaif, A. M., Maudlin, L. C., Crosbie, E.,  
711 Aghdam, M. A., Hossein Mardi, A., and Sorooshian, A.: Impact of wildfire emissions on  
712 chloride and bromide depletion in marine aerosol particles, *Environmental Science &*  
713 *Technology*, 51, 9013-9021, 2017.

714 Braun, R. A., Aghdam, M. A., Bañaga, P. A., Betito, G., Cambaliza, M. O., Cruz, M. T.,  
715 Lorenzo, G. R., MacDonald, A. B., Simpas, J. B., and Stahl, C.: Long-range aerosol transport  
716 and impacts on size-resolved aerosol composition in Metro Manila, Philippines, *Atmospheric*  
717 *Chemistry and Physics*, 20, 2387-2405, 2020.

718 Cao, Y., Zhang, Z., Xiao, H., Xie, Y., Liang, Y., and Xiao, H.: How aerosol pH responds to  
719 nitrate to sulfate ratio of fine-mode particulate, *Environmental Science and Pollution Research*,  
720 1-9, 2020.

721 Carranza, J., Fisher, B., Yoder, G., and Hahn, D.: On-line analysis of ambient air aerosols using  
722 laser-induced breakdown spectroscopy, *Spectrochimica Acta Part B: Atomic spectroscopy*, 56,  
723 851-864, 2001.

724 Chatterjee, A., Sarkar, C., Adak, A., Mukherjee, U., Ghosh, S., and Raha, S.: Ambient air quality  
725 during Diwali Festival over Kolkata-a mega-city in India, *Aerosol and Air Quality Research*, 13,  
726 1133-1144, 2013.

727 Cheng, Y., Engling, G., He, K.-b., Duan, F.-k., Du, Z.-y., Ma, Y.-l., Liang, L.-l., Lu, Z.-f., Liu,  
728 J.-m., and Zheng, M.: The characteristics of Beijing aerosol during two distinct episodes:  
729 Impacts of biomass burning and fireworks, *Environmental Pollution*, 185, 149-157, 2014.

730 Cohen, D. D., Stelcer, E., Santos, F. L., Prior, M., Thompson, C., and Pabroa, P. C.:  
731 Fingerprinting and source apportionment of fine particle pollution in Manila by IBA and PMF  
732 techniques: A 7-year study, *X-Ray Spectrometry: An International Journal*, 38, 18-25, 2009.

733 Crespo, J., Yubero, E., Nicolás, J. F., Lucarelli, F., Nava, S., Chiari, M., and Calzolari, G.: High-  
734 time resolution and size-segregated elemental composition in high-intensity pyrotechnic  
735 exposures, *Journal of hazardous materials*, 241, 82-91, 2012.

736 Crosbie, E., Sorooshian, A., Monfared, N. A., Shingler, T., and Esmaili, O.: A multi-year aerosol  
737 characterization for the greater Tehran area using satellite, surface, and modeling data,  
738 *Atmosphere*, 5, 178-197, 2014.

739 Cruz, M. T., Bañaga, P. A., Betito, G., Braun, R. A., Stahl, C., Aghdam, M. A., Cambaliza, M.  
740 O., Dadashazar, H., Hilario, M. R., and Lorenzo, G. R.: Size-resolved composition and  
741 morphology of particulate matter during the southwest monsoon in Metro Manila, Philippines,  
742 2019.

743 D'Anna, A.: *Kinetics of Soot Formation*, 2015.

744 de Leeuw, G., Cohen, L., Frohn, L. M., Geernaert, G., Hertel, O., Jensen, B., Jickells, T., Klein,  
745 L., Kunz, G. J., and Lund, S.: Atmospheric input of nitrogen into the North Sea: ANICE project  
746 overview, *Continental Shelf Research*, 21, 2073-2094, 2001.

747 Dela Piedra, M. C.: *A Filipino Tradition: The Role of Fireworks and Firecrackers in the*  
748 *Philippine Culture*, *TALA*, 1, 141-153, 2018.

749 Devara, P. C., Vijayakumar, K., Safai, P. D., Made, P. R., and Rao, P. S.: Celebration-induced  
750 air quality over a tropical urban station, Pune, India, *Atmospheric Pollution Research*, 6, 511-  
751 520, 2015.

752 Do, T.-M., Wang, C.-F., Hsieh, Y.-K., and Hsieh, H.-F.: Metals present in ambient air before and  
753 after a firework festival in Yanshui, Tainan, Taiwan, *Aerosol and Air Quality Research*, 12, 981-  
754 993, 2012.

755 Dorado, S. V., Holdsworth, J. L., Lagrosas, N. C., Villarin, J. R., Narisma, G., Ellis, J., and  
756 Perez, R.: Characterization of urban atmosphere of Manila with lidar, filter sampling, and  
757 radiosonde, *Lidar Remote Sensing for Industry and Environment Monitoring*, 2001, 591-598,  
758 Drewnick, F., Hings, S. S., Curtius, J., Eerdekens, G., and Williams, J.: Measurement of fine  
759 particulate and gas-phase species during the New Year's fireworks 2005 in Mainz, Germany,  
760 *Atmospheric Environment*, 40, 4316-4327, 2006.

761 Dusek, U., Frank, G., Curtius, J., Drewnick, F., Schneider, J., Kürten, A., Rose, D., Andreae, M.  
762 O., Borrmann, S., and Pöschl, U.: Enhanced organic mass fraction and decreased hygroscopicity  
763 of cloud condensation nuclei (CCN) during new particle formation events, *Geophysical Research*  
764 *Letters*, 37, 2010.

765 Dutcher, D. D., Perry, K. D., Cahill, T. A., and Copeland, S. A.: Effects of indoor pyrotechnic  
766 displays on the air quality in the Houston Astrodome, *Journal of the Air & Waste Management*  
767 *Association*, 49, 156-160, 1999.

768 Ennis, J. L., and Shanley, E. S.: On hazardous silver compounds, *Journal of Chemical Education*,  
769 68, A6, 1991.

770 Feng, J., Sun, P., Hu, X., Zhao, W., Wu, M., and Fu, J.: The chemical composition and sources  
771 of PM<sub>2.5</sub> during the 2009 Chinese New Year's holiday in Shanghai, *Atmospheric Research*,  
772 118, 435-444, 2012.

773 Gonzalez, M. E., Stahl, C., Cruz, M. T., Bañaga, P. A., Betito, G., Braun, R. A., Aghdam, M. A.,  
774 Cambaliza, M. O., Lorenzo, G. R., and MacDonald, A. B.: Contrasting the size-resolved nature  
775 of particulate arsenic, cadmium, and lead among diverse regions, *Atmospheric Pollution*  
776 *Research*, 2021.

777 Gysel, M., Crosier, J., Topping, D., Whitehead, J., Bower, K., Cubison, M., Williams, P., Flynn,  
778 M., McFiggans, G., and Coe, H.: Closure study between chemical composition and hygroscopic  
779 growth of aerosol particles during TORCH2, 2007.

780 Hersey, S. P., Craven, J. S., Metcalf, A. R., Lin, J., Latham, T., Suski, K. J., Cahill, J. F., Duong,  
781 H. T., Sorooshian, A., and Jonsson, H. H.: Composition and hygroscopicity of the Los Angeles  
782 aerosol: CalNex, *Journal of Geophysical Research: Atmospheres*, 118, 3016-3036, 2013.

783 Hilario, M. R. A., Cruz, M. T., Bañaga, P. A., Betito, G., Braun, R. A., Stahl, C., Cambaliza, M.  
784 O., Lorenzo, G. R., MacDonald, A. B., and AzadiAghdam, M.: Characterizing weekly cycles of  
785 particulate matter in a coastal megacity: The importance of a seasonal, size-resolved, and  
786 chemically-speciated analysis, *Journal of Geophysical Research: Atmospheres*, e2020JD032614,  
787 2020.

788 Hirai, K., Yamazaki, Y., Okada, K., FURUTA, S., and KUBO, K.: Acute eosinophilic  
789 pneumonia associated with smoke from fireworks, *Internal medicine*, 39, 401-403, 2000.

790 Hooper, W. P., and Eloranta, E. W.: Lidar measurements of wind in the planetary boundary  
791 layer: the method, accuracy and results from joint measurements with radiosonde and kytoon,  
792 *Journal of climate and applied meteorology*, 25, 990-1001, 1986.

793 Hopke, P. K., Cohen, D. D., Begum, B. A., Biswas, S. K., Ni, B., Pandit, G. G., Santoso, M.,  
794 Chung, Y.-S., Davy, P., and Markwitz, A.: Urban air quality in the Asian region, *Science of the*  
795 *Total Environment*, 404, 103-112, 2008.

796 Hussein, T., Dal Maso, M., Petaja, T., Koponen, I. K., Paatero, P., Aalto, P. P., Hameri, K., and  
797 Kulmala, M.: Evaluation of an automatic algorithm for fitting the particle number size  
798 distributions, *Boreal environment research*, 10, 337, 2005.

799 Jiang, Q., Sun, Y., Wang, Z., and Yin, Y.: Aerosol composition and sources during the Chinese  
800 Spring Festival: fireworks, secondary aerosol, and holiday effects, *ACPD*, 14, 20617-20646,  
801 2014.

802 Joly, A., Smargiassi, A., Kosatsky, T., Fournier, M., Dabek-Zlotorzynska, E., Celo, V., Mathieu,  
803 D., Servranckx, R., D'amours, R., and Malo, A.: Characterisation of particulate exposure during  
804 fireworks displays, *Atmospheric Environment*, 44, 4325-4329, 2010.

805 Joshi, M., Khan, A., Anand, S., and Sapra, B.: Size evolution of ultrafine particles: Differential  
806 signatures of normal and episodic events, *Environmental pollution*, 208, 354-360, 2016.

807 Joshi, M., Nakhwa, A., Khandare, P., Khan, A., and Sapra, B.: Simultaneous measurements of  
808 mass, chemical compositional and number characteristics of aerosol particles emitted during  
809 fireworks, *Atmospheric Environment*, 217, 116925, 2019.

810 Karnae, S.: Analysis of aerosol composition and characteristics in a semi arid coastal urban area,  
811 Texas A&M University-Kingsville, 2005.

812 Khaparde, V. V., Pipalatkhar, P. P., Pustode, T., Rao, C. C., and Gajghate, D. G.: Influence of  
813 burning of fireworks on particle size distribution of PM 10 and associated barium at Nagpur,  
814 *Environmental monitoring and assessment*, 184, 903-911, 2012.

815 Kong, S., Li, L., Li, X., Yin, Y., Chen, K., Liu, D., Yuan, L., Zhang, Y., Shan, Y., and Ji, Y.: The  
816 impacts of firework burning at the Chinese Spring Festival on air quality: insights of tracers,  
817 source evolution and aging processes, *Atmos. Chem. Phys.*, 15, 2167-2184, 2015.

818 Kulshrestha, U., Rao, T. N., Azhaguvel, S., and Kulshrestha, M.: Emissions and accumulation of  
819 metals in the atmosphere due to crackers and sparkles during Diwali festival in India,  
820 *Atmospheric Environment*, 38, 4421-4425, 2004.

821 Kumar, M., Singh, R., Murari, V., Singh, A., Singh, R., and Banerjee, T.: Fireworks induced  
822 particle pollution: a spatio-temporal analysis, *Atmospheric research*, 180, 78-91, 2016.

823 Lai, Y., and Brimblecombe, P.: Changes in air pollution and attitude to fireworks in Beijing,  
824 *Atmospheric Environment*, 117549, 2020.

825 Li, J., Xu, T., Lu, X., Chen, H., Nizkorodov, S. A., Chen, J., Yang, X., Mo, Z., Chen, Z., and  
826 Liu, H.: Online single particle measurement of fireworks pollution during Chinese New Year in  
827 Nanning, *Journal of Environmental Sciences*, 53, 184-195, 2017.

828 Licudine, J. A., Yee, H., Chang, W. L., and Whelen, A. C.: Hazardous metals in ambient air due  
829 to New Year fireworks during 2004–2011 celebrations in Pearl City, Hawaii, *Public Health*  
830 *Reports*, 127, 440-450, 2012.

831 Lin, C.-C.: A review of the impact of fireworks on particulate matter in ambient air, *Journal of*  
832 *the Air & Waste Management Association*, 66, 1171-1182, 2016.

833 Lin, C.-C., Yang, L.-S., and Cheng, Y.-H.: Ambient PM<sub>2.5</sub>, black carbon, and particle size-  
834 resolved number concentrations and the Ångström exponent value of aerosols during the  
835 firework display at the lantern festival in southern Taiwan, *Aerosol Air Qual. Res.*, 16, 373-387,  
836 2016.

837 Liu, D.-Y., Rutherford, D., Kinsey, M., and Prather, K. A.: Real-time monitoring of  
838 pyrotechnically derived aerosol particles in the troposphere, *Analytical Chemistry*, 69, 1808-  
839 1814, 1997.

840 Marple, V., Olson, B., Romay, F., Hudak, G., Geerts, S. M., and Lundgren, D.: Second  
841 generation micro-orifice uniform deposit impactor, 120 MOUDI-II: Design, evaluation, and  
842 application to long-term ambient sampling, *Aerosol Science and Technology*, 48, 427-433, 2014.  
843 Martín-Alberca, C., and García-Ruiz, C.: Analytical techniques for the analysis of consumer  
844 fireworks, *TrAC Trends in Analytical Chemistry*, 56, 27-36, 2014.  
845 Martín-Alberca, C., Zapata, F., Carrascosa, H., Ortega-Ojeda, F. E., and García-Ruiz, C.: Study  
846 of consumer fireworks post-blast residues by ATR-FTIR, *Talanta*, 149, 257-265, 2016.  
847 Mönkkönen, P., Uma, R., Srinivasan, D., Koponen, I., Lehtinen, K., Hämeri, K., Suresh, R.,  
848 Sharma, V., and Kulmala, M.: Relationship and variations of aerosol number and PM10 mass  
849 concentrations in a highly polluted urban environment—New Delhi, India, *Atmospheric*  
850 *Environment*, 38, 425-433, 2004.  
851 Mora, M., Braun, R. A., Shingler, T., and Sorooshian, A.: Analysis of remotely sensed and  
852 surface data of aerosols and meteorology for the Mexico Megalopolis Area between 2003 and  
853 2015, *Journal of Geophysical Research: Atmospheres*, 122, 8705-8723, 2017.  
854 Moreno, T., Querol, X., Alastuey, A., Amato, F., Pey, J., Pandolfi, M., Kuenzli, N., Bouso, L.,  
855 Rivera, M., and Gibbons, W.: Effect of fireworks events on urban background trace metal  
856 aerosol concentrations: is the cocktail worth the show?, *Journal of hazardous materials*, 183, 945-  
857 949, 2010.  
858 Nicolás, J., Yubero, E., Galindo, N., Giménez, J., Castañer, R., Carratalá, A., Crespo, J., and  
859 Pastor, C.: Characterization of events by aerosol mass size distributions, *Journal of*  
860 *Environmental Monitoring*, 11, 394-399, 2009.  
861 Oanh, N. K., Upadhyay, N., Zhuang, Y.-H., Hao, Z.-P., Murthy, D., Lestari, P., Villarin, J.,  
862 Chengchua, K., Co, H., and Dung, N.: Particulate air pollution in six Asian cities: Spatial and  
863 temporal distributions, and associated sources, *Atmospheric environment*, 40, 3367-3380, 2006.  
864 Perrino, C., Tiwari, S., Catrambone, M., Dalla Torre, S., Rantica, E., and Canepari, S.: Chemical  
865 characterization of atmospheric PM in Delhi, India, during different periods of the year including  
866 Diwali festival, *Atmospheric Pollution Research*, 2, 418-427, 2011.  
867 Perry, K. D.: Effects of outdoor pyrotechnic displays on the regional air quality of Western  
868 Washington State, *Journal of the Air & Waste Management Association*, 49, 146-155, 1999.  
869 Petters, M., and Kreidenweis, S.: A single parameter representation of hygroscopic growth and  
870 cloud condensation nucleus activity, *Atmospheric Chemistry and Physics*, 7, 1961-1971, 2007.  
871 Pirker, L., Gradišek, A., Višić, B., and Remškar, M.: Nanoparticle exposure due to pyrotechnics  
872 during a football match, *Atmospheric Environment*, 117567, 2020.  
873 Pósfai, M., Simonics, R., Li, J., Hobbs, P. V., and Buseck, P. R.: Individual aerosol particles  
874 from biomass burning in southern Africa: 1. Compositions and size distributions of carbonaceous  
875 particles, *Journal of Geophysical Research: Atmospheres*, 108, 2003.  
876 Prospero, J. M., Savoie, D. L., and Arimoto, R.: Long-term record of nss-sulfate and nitrate in  
877 aerosols on Midway Island, 1981–2000: Evidence of increased (now decreasing?) anthropogenic  
878 emissions from Asia, *Journal of Geophysical Research: Atmospheres*, 108, AAC 10-11-AAC 10-  
879 11, 2003.  
880 PSA: NCR Statistics: <http://rssoncr.psa.gov.ph/>, access: February 13, 2021, 2015.  
881 Rao, P. S., Gajghate, D., Gavane, A., Suryawanshi, P., Chauhan, C., Mishra, S., Gupta, N., Rao,  
882 C., and Wate, S.: Air quality status during Diwali Festival of India: A case study, *Bulletin of*  
883 *environmental contamination and toxicology*, 89, 376-379, 2012.  
884 Ravindra, K., Mor, S., and Kaushik, C.: Short-term variation in air quality associated with  
885 firework events: a case study, *Journal of Environmental Monitoring*, 5, 260-264, 2003.

886 Razenkov, I.: Characterization of a Geiger-mode avalanche photodiode detector for high spectral  
887 resolution lidar, University of Wisconsin--Madison, 2010.

888 Reid, J. S., Hyer, E. J., Johnson, R. S., Holben, B. N., Yokelson, R. J., Zhang, J., Campbell, J. R.,  
889 Christopher, S. A., Di Girolamo, L., and Giglio, L.: Observing and understanding the Southeast  
890 Asian aerosol system by remote sensing: An initial review and analysis for the Seven Southeast  
891 Asian Studies (7SEAS) program, *Atmospheric Research*, 122, 403-468, 2013.

892 Retama, A., Neria-Hernández, A., Jaimes-Palomera, M., Rivera-Hernández, O., Sánchez-  
893 Rodríguez, M., López-Medina, A., and Velasco, E.: Fireworks: a major source of inorganic and  
894 organic aerosols during Christmas and New Year in Mexico city, *Atmospheric Environment: X*,  
895 2, 100013, 2019.

896 Roca, J. B., de Los Reyes, V. C., Racelis, S., Deveraturda, I., Sualdito, M. N., Tayag, E., and  
897 O'Reilly, M.: Fireworks-related injury surveillance in the Philippines: trends in 2010–2014,  
898 *Western Pacific surveillance and response journal: WPSAR*, 6, 1, 2015.

899 Rolph, G., Stein, A., and Stunder, B.: Real-time environmental applications and display system:  
900 READY, *Environmental Modelling & Software*, 95, 210-228, 2017.

901 Santos, F. L., Pabroa, P. C. B., Morco, R. P., and Racho, J. M. D.: Elemental characterization of  
902 New Year's Day PM10 and PM2. 2 particulates matter at several sites in Metro Manila, *Book of*  
903 *abstracts*, 2007,

904 Santos Flora, L., Pabroa, C. B., Morco, R. P., and Racho, J. M. D.: Elemental characterization of  
905 inhalable particulate emissions on New Year's day in Metro Manila, *Philippines Nuclear Journal*,  
906 15, 35-43, 2010.

907 Sarkar, S., Khillare, P. S., Jyethi, D. S., Hasan, A., and Parween, M.: Chemical speciation of  
908 respirable suspended particulate matter during a major firework festival in India, *Journal of*  
909 *Hazardous Materials*, 184, 321-330, 2010.

910 Schlosser, J. S., Braun, R. A., Bradley, T., Dadashazar, H., MacDonald, A. B., Aldhaif, A. A.,  
911 Aghdam, M. A., Mardi, A. H., Xian, P., and Sorooshian, A.: Analysis of aerosol composition  
912 data for western United States wildfires between 2005 and 2015: Dust emissions, chloride  
913 depletion, and most enhanced aerosol constituents, *Journal of Geophysical Research:*  
914 *Atmospheres*, 122, 8951-8966, 2017.

915 Shen, Z., Cao, J., Arimoto, R., Han, Z., Zhang, R., Han, Y., Liu, S., Okuda, T., Nakao, S., and  
916 Tanaka, S.: Ionic composition of TSP and PM2. 5 during dust storms and air pollution episodes  
917 at Xi'an, China, *Atmospheric Environment*, 43, 2911-2918, 2009.

918 Shimizu, T.: *Fireworks: the art, science, and technique*, Pyrotechnica publications, 1988.

919 Shingler, T., Crosbie, E., Ortega, A., Shiraiwa, M., Zuend, A., Beyersdorf, A., Ziemba, L.,  
920 Anderson, B., Thornhill, L., and Perring, A. E.: Airborne characterization of subsaturated aerosol  
921 hygroscopicity and dry refractive index from the surface to 6.5 km during the SEAC4RS  
922 campaign, *Journal of Geophysical Research: Atmospheres*, 121, 4188-4210, 2016.

923 Shinozuka, Y., Clarke, A., DeCarlo, P., Jimenez, J., Dunlea, E., Roberts, G., Tomlinson, J.,  
924 Collins, D., Howell, S., and Kapustin, V.: Aerosol optical properties relevant to regional remote  
925 sensing of CCN activity and links to their organic mass fraction: airborne observations over  
926 Central Mexico and the US West Coast during MILAGRO/INTEX-B, 1foldr Import 2019-10-08  
927 Batch 9, 2009.

928 Singh, A., Pant, P., and Pope, F. D.: Air quality during and after festivals: Aerosol  
929 concentrations, composition and health effects, *Atmospheric Research*, 2019.

930 Stahl, C., Cruz, M. T., Bañaga, P. A., Betito, G., Braun, R. A., Aghdam, M. A., Cambaliza, M.  
931 O., Lorenzo, G. R., MacDonald, A. B., Pabroa, P. C., Yee, J. R., Simpas, J. B., and Sorooshian,



932 A.: An annual time series of weekly size-resolved aerosol properties in the megacity of Metro  
933 Manila, Philippines, *Scientific Data*, 7, 128, 10.1038/s41597-020-0466-y, 2020b.

934 Stein, A., Draxler, R. R., Rolph, G. D., Stunder, B. J., Cohen, M., and Ngan, F.: NOAA's  
935 HYSPLIT atmospheric transport and dispersion modeling system, *Bulletin of the American*  
936 *Meteorological Society*, 96, 2059-2077, 2015.

937 Steinhauser, G., and Klapotke, T. M.: Using the chemistry of fireworks to engage students in  
938 learning basic chemical principles: a lesson in eco-friendly pyrotechnics, *Journal of Chemical*  
939 *Education*, 87, 150-156, 2010.

940 Stokes, R., and Robinson, R.: Interactions in aqueous nonelectrolyte solutions. I. Solute-solvent  
941 equilibria, *The Journal of Physical Chemistry*, 70, 2126-2131, 1966.

942 Sun, Y., Wang, Z., Fu, P., Jiang, Q., Yang, T., Li, J., and Ge, X.: The impact of relative humidity  
943 on aerosol composition and evolution processes during wintertime in Beijing, China,  
944 *Atmospheric Environment*, 77, 927-934, 2013.

945 Tanda, S., Ličbinský, R., Hegrová, J., and Goessler, W.: Impact of New Year's Eve fireworks on  
946 the size resolved element distributions in airborne particles, *Environment international*, 128, 371-  
947 378, 2019.

948 ten Brink, H., Henzing, B., Otjes, R., and Weijers, E.: Visibility in the Netherlands during New  
949 Year's fireworks: The role of soot and salty aerosol products, *Atmospheric Environment*, 173,  
950 289-294, 2018.

951 Thakur, B., Chakraborty, S., Debsarkar, A., Chakrabarty, S., and Srivastava, R.: Air pollution  
952 from fireworks during festival of lights (Deepawali) in Howrah, India-a case study, *Atmosfera*,  
953 23, 347-365, 2010.

954 Tian, Y., Wang, J., Peng, X., Shi, G., and Feng, Y.: Estimation of the direct and indirect impacts  
955 of fireworks on the physicochemical characteristics of atmospheric PM10 and PM2. 5,  
956 *Atmospheric Chemistry and Physics*, 9469, 2014.

957 Totsuka, T., Sase, H., and Shimizu, H.: Major activities of acid deposition monitoring network in  
958 East Asia (EANET) and related studies, in: *Plant Responses to Air Pollution and Global Change*,  
959 Springer, 251-259, 2005.

960 Tsai, H.-H., Chien, L.-H., Yuan, C.-S., Lin, Y.-C., Jen, Y.-H., and Ie, I.-R.: Influences of  
961 fireworks on chemical characteristics of atmospheric fine and coarse particles during Taiwan's  
962 Lantern Festival, *Atmospheric Environment*, 62, 256-264, 2012.

963 Tsai, J.-H., Lin, J.-H., Yao, Y.-C., and Chiang, H.-L.: Size distribution and water soluble ions of  
964 ambient particulate matter on episode and non-episode days in Southern Taiwan, *Aerosol and*  
965 *Air Quality Research*, 12, 263-274, 2011.

966 Tsay, S.-C., Hsu, N. C., Lau, W. K.-M., Li, C., Gabriel, P. M., Ji, Q., Holben, B. N., Welton, E.  
967 J., Nguyen, A. X., and Janjai, S.: From BASE-ASIA toward 7-SEAS: A satellite-surface  
968 perspective of boreal spring biomass-burning aerosols and clouds in Southeast Asia,  
969 *Atmospheric environment*, 78, 20-34, 2013.

970 Vecchi, R., Bernardoni, V., Cricchio, D., D'Alessandro, A., Fermo, P., Lucarelli, F., Nava, S.,  
971 Piazzalunga, A., and Valli, G.: The impact of fireworks on airborne particles, *Atmospheric*  
972 *Environment*, 42, 1121-1132, 2008.

973 Villafuerte II, M. Q., Matsumoto, J., Akasaka, I., Takahashi, H. G., Kubota, H., and Cinco, T. A.:  
974 Long-term trends and variability of rainfall extremes in the Philippines, *Atmospheric Research*,  
975 137, 1-13, 2014.

976 Walsh, K. J., Milligan, M., and Sherwell, J.: Synoptic evaluation of regional PM2. 5  
977 concentrations, *Atmospheric Environment*, 43, 594-603, 2009.

978 Wang, Y., Zhuang, G., Xu, C., and An, Z.: The air pollution caused by the burning of fireworks  
979 during the lantern festival in Beijing, *Atmospheric Environment*, 41, 417-431, 2007.

980 Wehner, B., Wiedensohler, A., and Heintzenberg, J.: Submicrometer aerosol size distributions  
981 and mass concentration of the millennium fireworks 2000 in Leipzig, Germany, *Journal of*  
982 *Aerosol Science*, 12, 1489-1493, 2000.

983 Wilkin, R. T., Fine, D. D., and Burnett, N. G.: Perchlorate behavior in a municipal lake  
984 following fireworks displays, *Environmental Science & Technology*, 41, 3966-3971, 2007.

985 Wonaschuetz, A., Sorooshian, A., Ervens, B., Chuang, P. Y., Feingold, G., Murphy, S. M., De  
986 Gouw, J., Warneke, C., and Jonsson, H. H.: Aerosol and gas re-distribution by shallow cumulus  
987 clouds: An investigation using airborne measurements, *Journal of Geophysical Research:*  
988 *Atmospheres*, 117, 2012.

989 Wu, C., Wang, G., Wang, J., Li, J., Ren, Y., Zhang, L., Cao, C., Li, J., Ge, S., and Xie, Y.:  
990 Chemical characteristics of haze particles in Xi'an during Chinese Spring Festival: Impact of  
991 fireworks burning, *Journal of Environmental Sciences*, 71, 179-187, 2018.

992 Yadav, S. K., Kumar, M., Sharma, Y., Shukla, P., Singh, R. S., and Banerjee, T.: Temporal  
993 evolution of submicron particles during extreme fireworks, *Environmental monitoring and*  
994 *assessment*, 191, 576, 2019.

995 Yang, L., Gao, X., Wang, X., Nie, W., Wang, J., Gao, R., Xu, P., Shou, Y., Zhang, Q., and  
996 Wang, W.: Impacts of firecracker burning on aerosol chemical characteristics and human health  
997 risk levels during the Chinese New Year Celebration in Jinan, China, *Science of the Total*  
998 *Environment*, 476, 57-64, 2014.

999 Youn, J. S., Wang, Z., Wonaschütz, A., Arellano, A., Betterton, E. A., and Sorooshian, A.:  
1000 Evidence of aqueous secondary organic aerosol formation from biogenic emissions in the North  
1001 American Sonoran Desert, *Geophysical research letters*, 40, 3468-3472, 2013.

1002 Yuan, L., Zhang, X., Feng, M., Liu, X., Che, Y., Xu, H., Schaefer, K., Wang, S., and Zhou, Y.:  
1003 Size-resolved hygroscopic behaviour and mixing state of submicron aerosols in a megacity of the  
1004 Sichuan Basin during pollution and fireworks episodes, *Atmospheric Environment*, 226, 117393,  
1005 2020.

1006 Zhang, J., Yang, L., Chen, J., Mellouki, A., Jiang, P., Gao, Y., Li, Y., Yang, Y., and Wang, W.:  
1007 Influence of fireworks displays on the chemical characteristics of PM<sub>2.5</sub> in rural and suburban  
1008 areas in Central and East China, *Science of the Total Environment*, 578, 476-484, 2017.

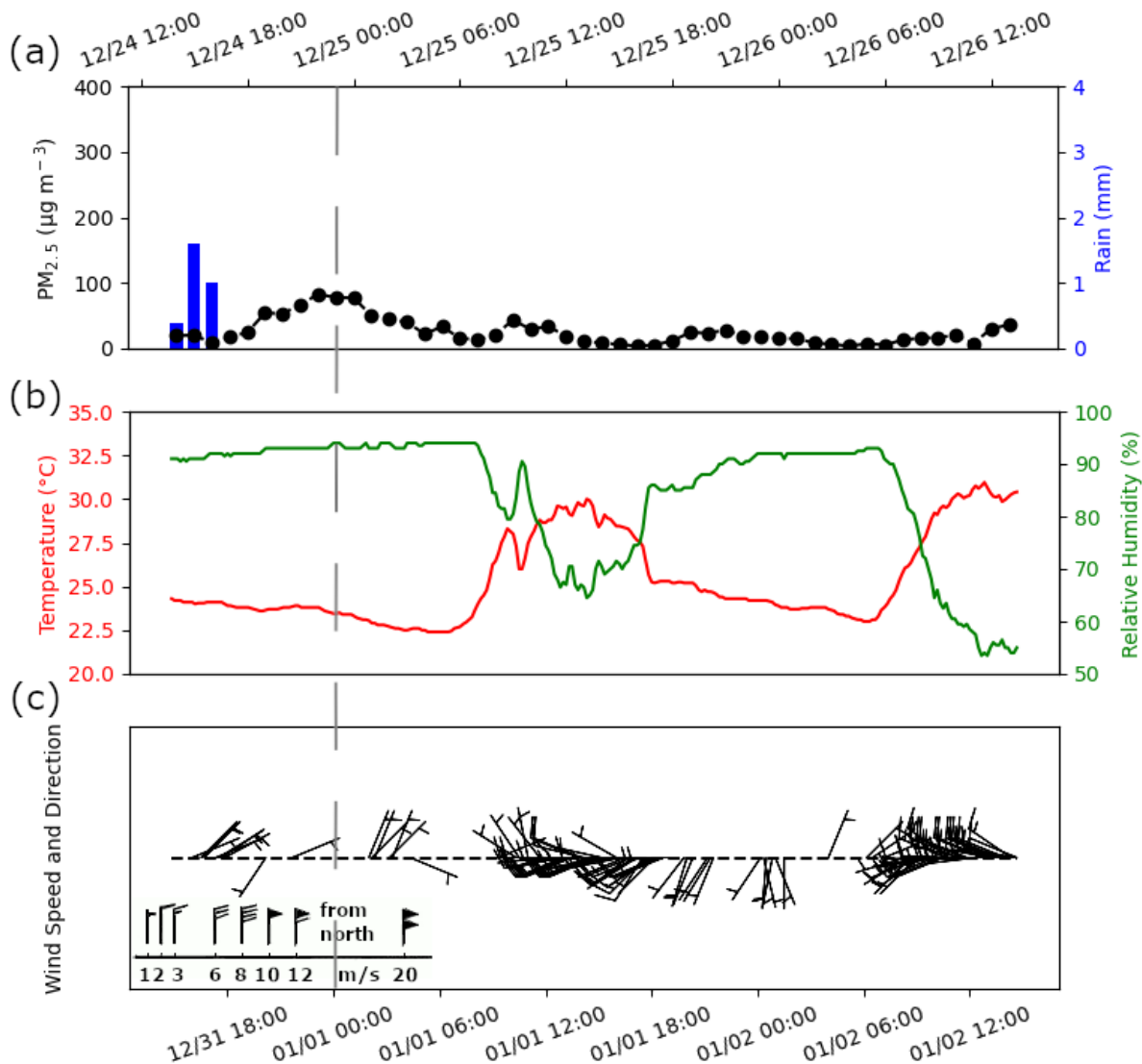
1009 Zhang, J., Lance, S., Freedman, J. M., Sun, Y., Crandall, B. A., Wei, X., and Schwab, J. J.:  
1010 Detailed Measurements of Submicron Particles from an Independence Day Fireworks Event in  
1011 Albany, New York Using HR-ToF-AMS, *ACS Earth and Space Chemistry*, 3, 1451-1459, 2019.

1012 Zhang, M., Wang, X., Chen, J., Cheng, T., Wang, T., Yang, X., Gong, Y., Geng, F., and Chen,  
1013 C.: Physical characterization of aerosol particles during the Chinese New Year's firework events,  
1014 *Atmospheric Environment*, 44, 5191-5198, 2010.

1015 **Table 1:** Summary of total and speciated concentrations before, during, and after the firework  
 1016 event. Species are divided based on units (Total to Zn:  $\mu\text{g m}^{-3}$ ; succinate to Se:  $\text{ng m}^{-3}$ ).

Species	Total Concentration			Species	Total Concentration		
	Before	During	After		Before	During	After
<b>TOTAL</b>	2.93	16.74	3.54	<b>MSA</b>	4.44	3.22	2.43
<b>nss-SO<sub>4</sub><sup>2-</sup></b>	0.73	6.81	0.66	<b>Mn</b>	0.88	2.97	1.03
<b>K<sup>+</sup></b>	0.37	5.05	0.25	<b>Rb</b>	0.62	1.24	0.25
<b>NO<sub>3</sub><sup>-</sup></b>	0.64	1.70	0.65	<b>Cr</b>	0.16	1.01	0.29
<b>Cl<sup>-</sup></b>	0.23	1.46	0.57	<b>As</b>	0.60	0.71	0.38
<b>Mg<sup>2+</sup></b>	0.06	0.37	0.10	<b>Ni</b>	0.41	0.46	0.99
<b>Na<sup>+</sup></b>	0.33	0.33	0.53	<b>Ti</b>	0.10	0.27	0.24
<b>Ca<sup>2+</sup></b>	0.21	0.30	0.38	<b>V</b>	0.32	0.14	0.30
<b>NH<sub>4</sub><sup>+</sup></b>	0.21	0.19	0.28	<b>Mo</b>	0.05	0.10	0.06
<b>Ba</b>	0.01	0.17	0.01	<b>Cd</b>	0.11	0.10	0.13
<b>oxalate</b>	0.10	0.12	0.06	<b>Co</b>	0.05	0.05	0.05
<b>Cu</b>	2.48E-04	6.89E-02	1.86E-03	<b>Cs</b>	0.02	0.02	0.01
<b>Al</b>	4.53E-03	0.05	0.01	<b>Ag</b>	0.02	0.02	4.00E-04
<b>Sr</b>	1.27E-03	4.65E-02	2.54E-03	<b>Tl</b>	0.01	0.02	1.80E-03
<b>Zn</b>	0.01	0.02	0.01	<b>Zr</b>	0.01	0.01	0.03
<b>succinate</b>	0.98	9.51	0	<b>Sn</b>	0.01	6.69E-04	0.03
<b>Pb</b>	1.68	8.33	1.03	<b>Y</b>	2.16E-04	4.56E-04	2.44E-03
<b>phthalate</b>	12.82	5.36	5.59	<b>Nb</b>	2.28E-04	1.59E-04	3.00E-04
<b>adipate</b>	5.35	4.83	11.73	<b>Hf</b>	0	0	2.18E-04
<b>maleate</b>	1.54	4.12	0	<b>Hg</b>	1.03E-03	0	0
<b>Fe</b>	2.91	3.47	7.32	<b>Se</b>	5.76	0	0

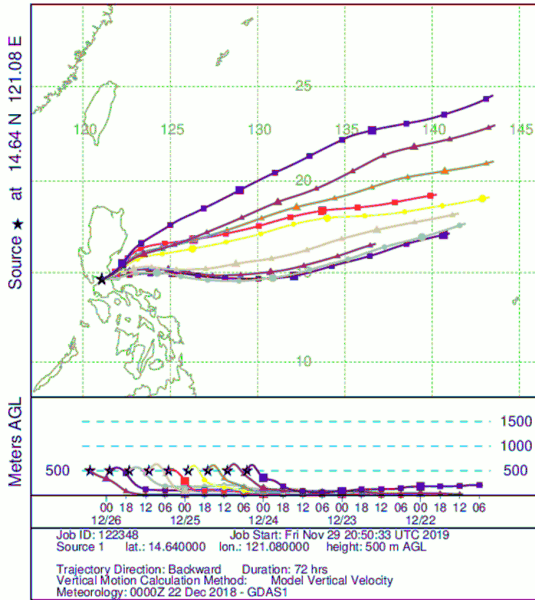
1017



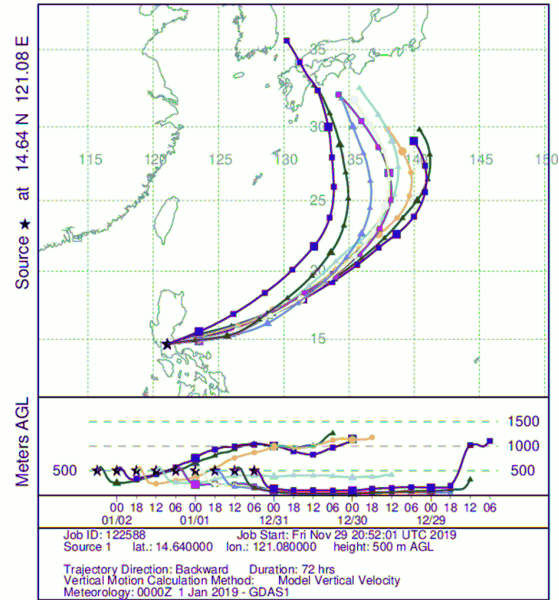
1018

1019 **Figure 1:** (a) PM<sub>2.5</sub> mass concentrations and rain accumulation at hourly resolution (local time,  
 1020 dashed vertical line indicates midnight) as measured from the Manila Observatory main building  
 1021 third floor rooftop (~88 m.a.s.l.) at the same period as the MOUDI size-specified samples during  
 1022 the firework event. Ten-minute averaged values of (b) temperature and relative humidity, in  
 1023 addition to (c) wind speed and direction. The wind barb legend in (c) shows how flags are added  
 1024 to the staff with increasing wind speed and in the direction where the wind comes from. Figures  
 1025 S2 and S3 show the hourly PM<sub>2.5</sub> mass concentrations and ten-minute meteorological data before  
 1026 and after the firework event, respectively.

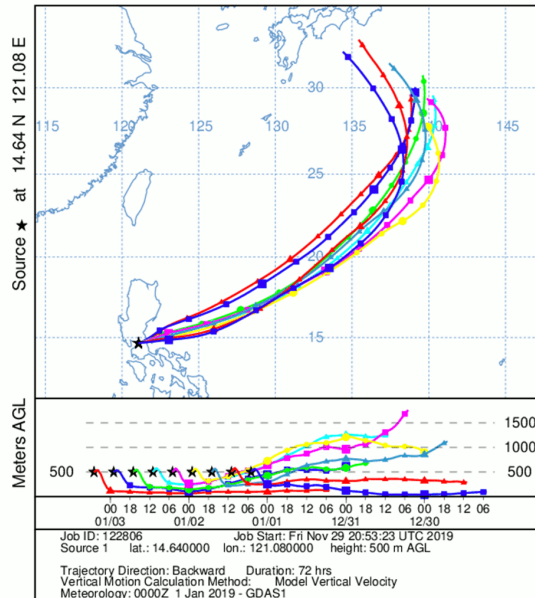
(a) NOAA HYSPLIT MODEL  
Backward trajectories ending at 0500 UTC 26 Dec 18  
GDAS Meteorological Data



(b) NOAA HYSPLIT MODEL  
Backward trajectories ending at 0600 UTC 02 Jan 19  
GDAS Meteorological Data



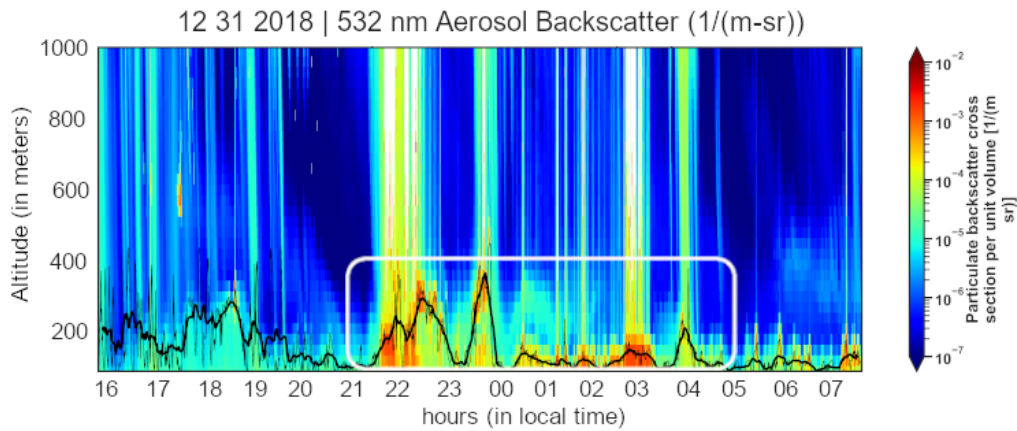
(c) NOAA HYSPLIT MODEL  
Backward trajectories ending at 0500 UTC 03 Jan 19  
GDAS Meteorological Data



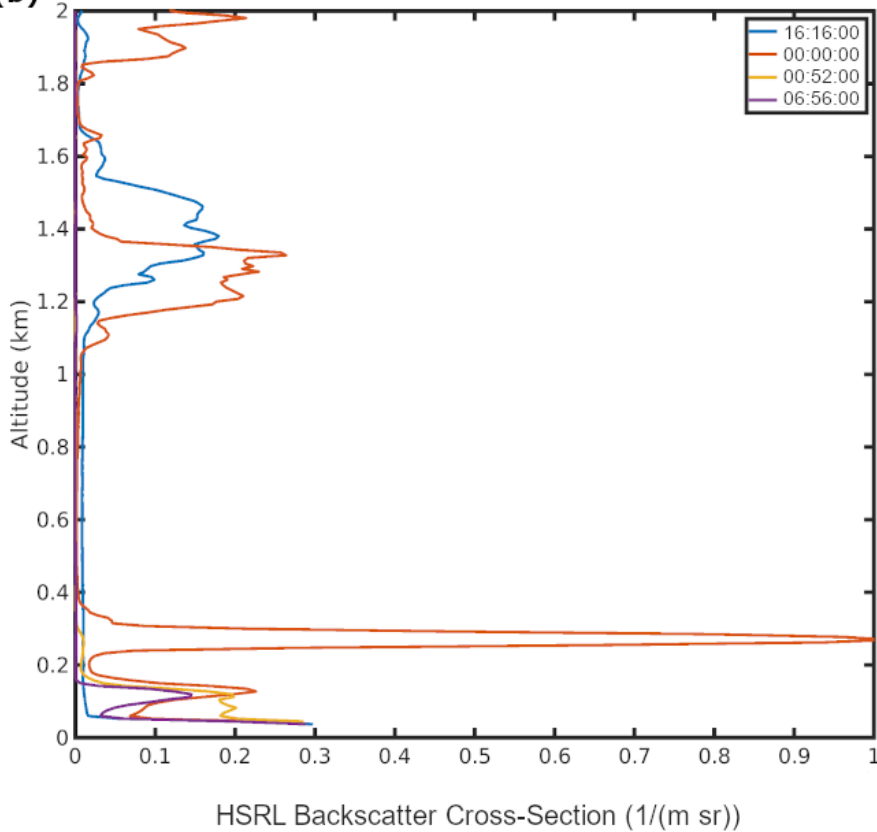
1027

1028 **Figure 2:** Three-day back trajectories with 6-h resolution for the periods (a) before, (b) during,  
1029 and (c) after the firework event, ending at the point of the Manila Observatory at 500 m.

(a)



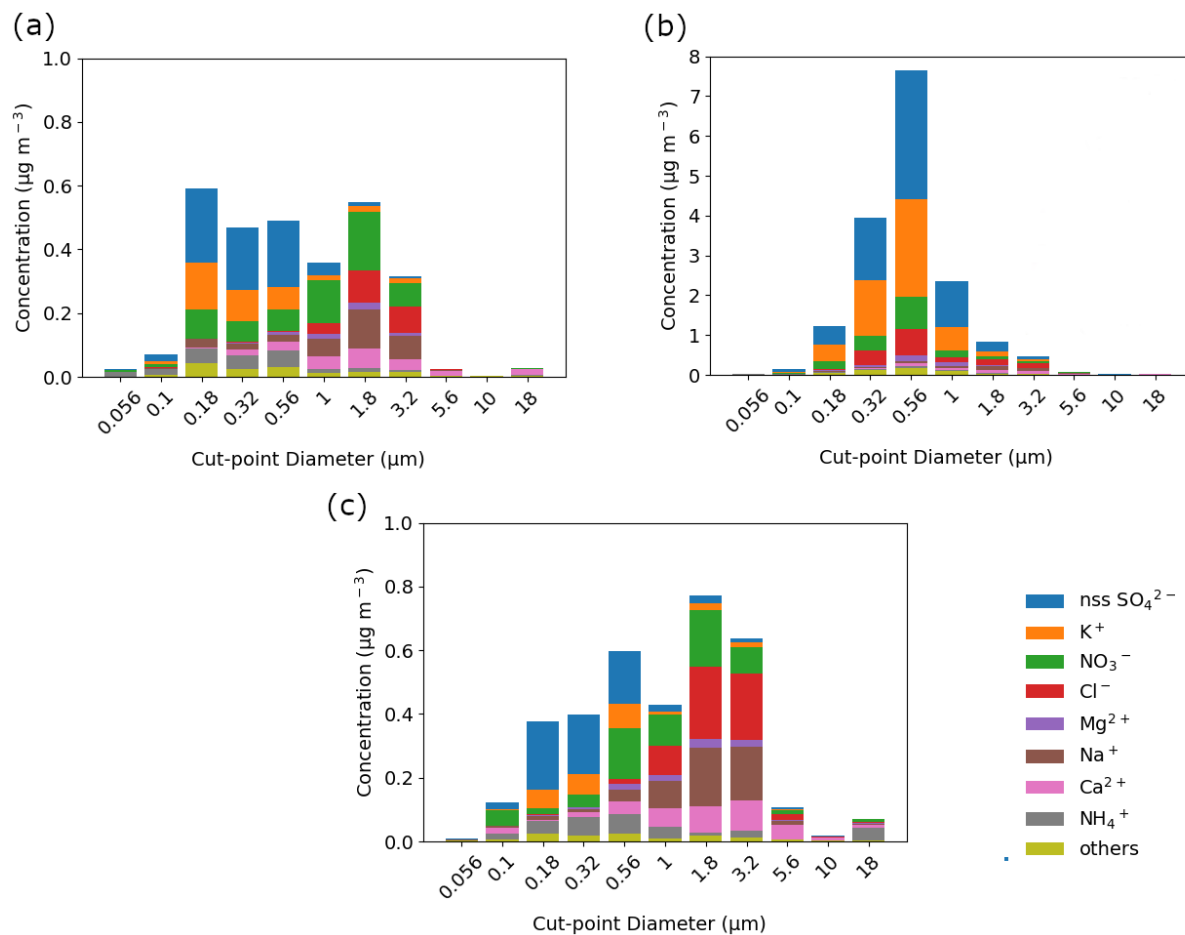
(b)



1030

1031 **Figure 3:** (a) Time series of the aerosol backscatter vertical profile from the High Spectral  
1032 Resolution Layer (HSRL). The time shown is Universal Time (UT) and local time is UT + 8  
1033 hours. The times circled by the white oval correspond to the peak of aerosol backscatter in the  
1034 mixing layer due to firework activity. The approximate surface-attached aerosol layer height is  
1035 shown as a thick black line. It is derived from a 30-min moving window average based on the 1-  
1036 min values shown in thin black line (b) Vertical profiles of aerosol back-scatter at specific UT  
1037 times of interest before, during, and after the fireworks.

1038



1040

1041

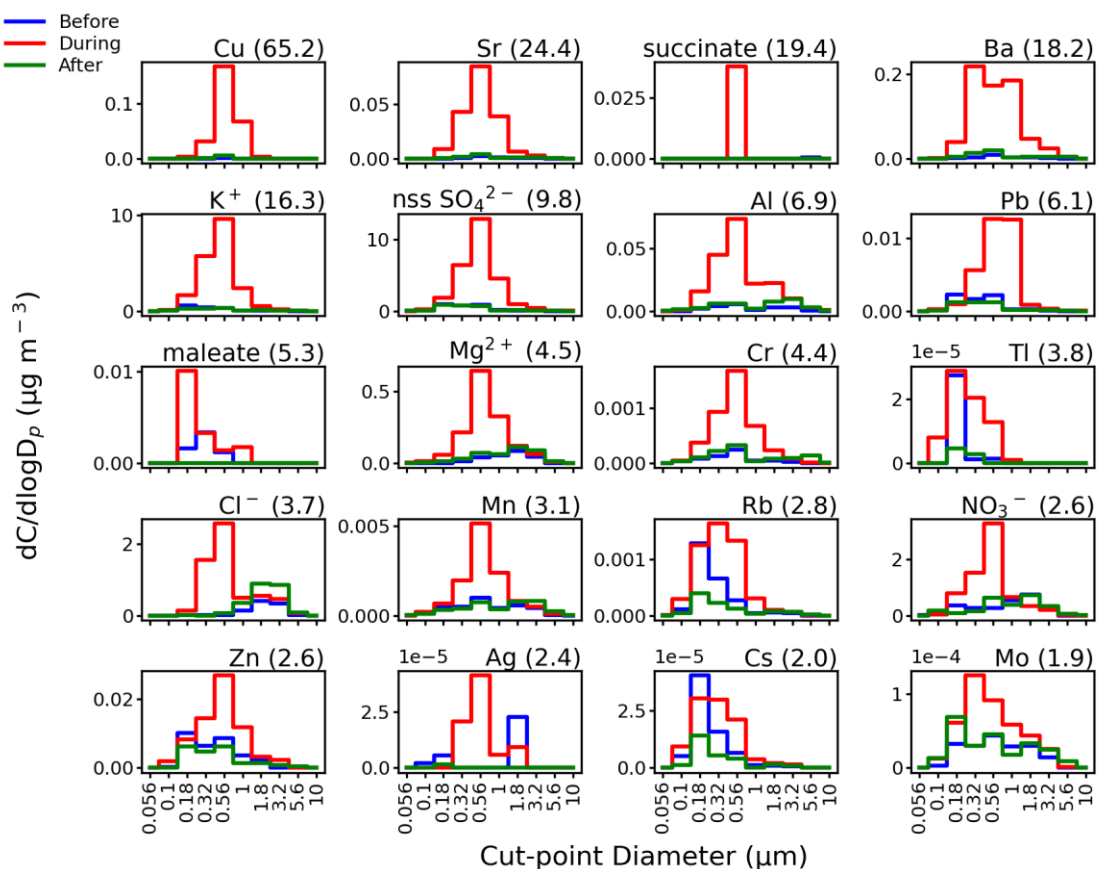
1042

1043

1044

1045

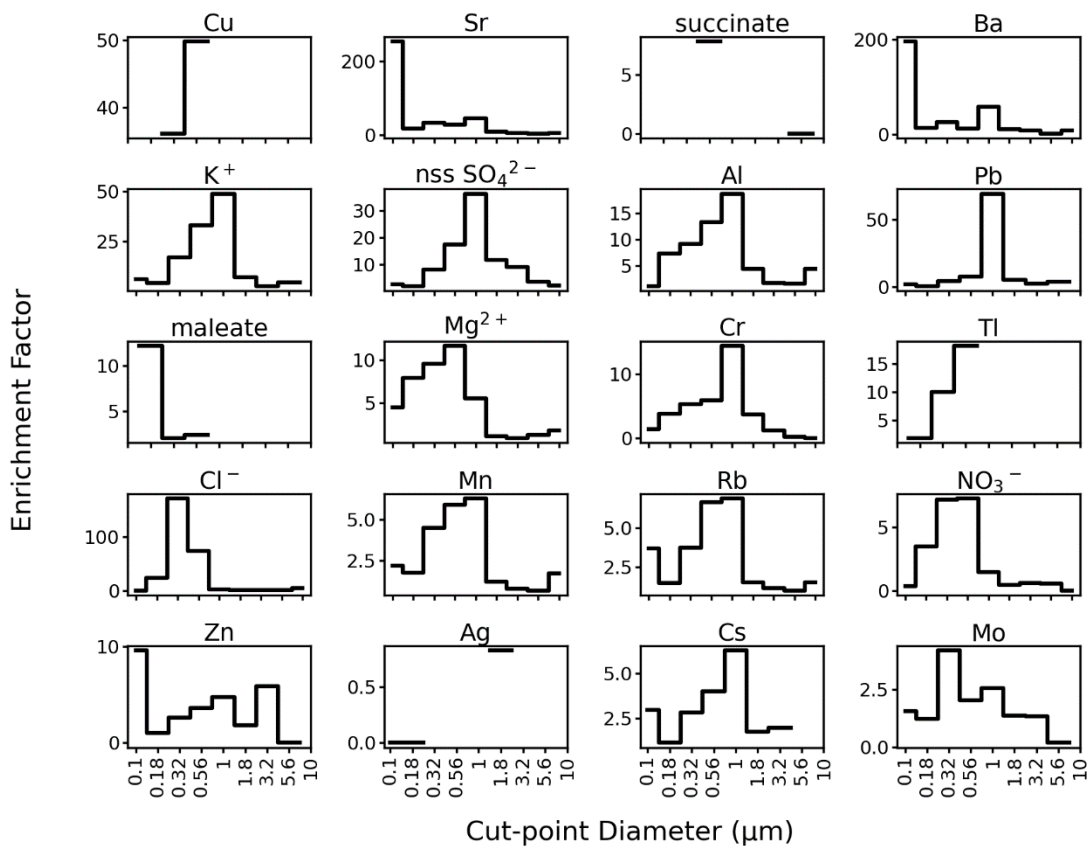
**Figure 4:** Speciated mass size distributions of the major aerosol constituents measured (a) before, (b) during, and (c) after the firework event. Table 1 lists the bulk ( $\geq 0.056 \mu\text{m}$ ) mass concentrations of these ions and elements, including those labeled here as “others” (Ba, oxalate, Cu, Al, Sr, Zn, succinate, Pb, phthalate, adipate, maleate, Fe, MSA, Mn, Rb, Cr, As, Ni, Ti, V, Mo, Cd, Co, Cs, Ag, Tl, Zr, Sn, Y, Nb, Hf, Hg, and Se).



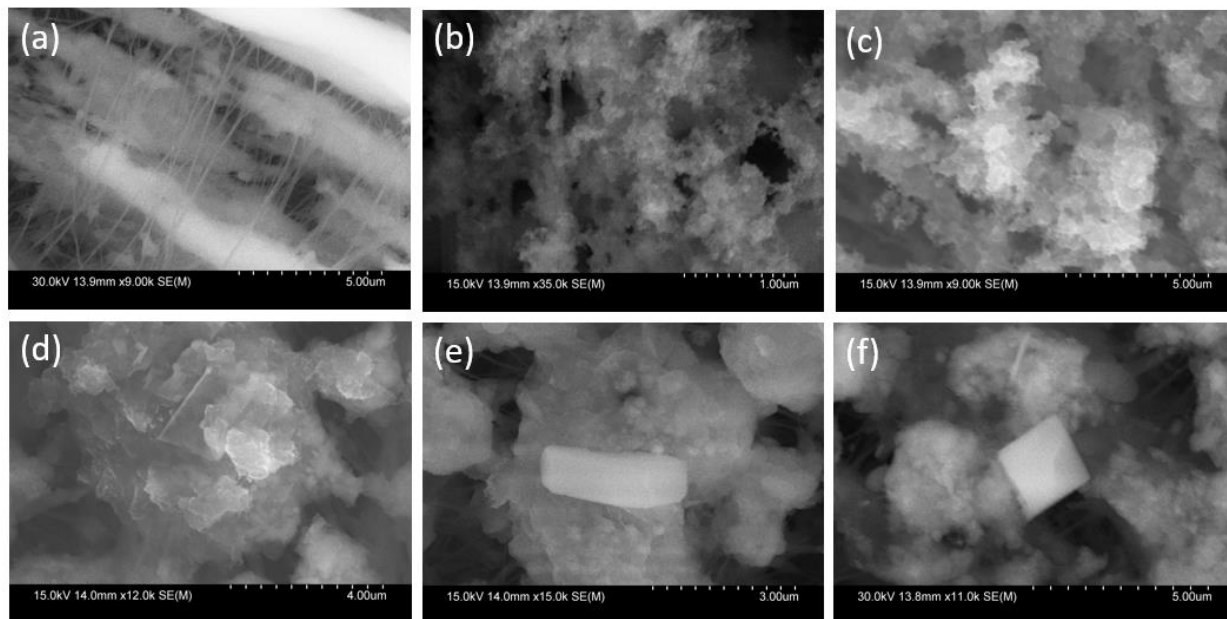
1046

1047 **Figure 5:** Speciated mass size distributions before (blue line), during (red line), and after (green line)  
 1048 the firework event. Next to species labels are bulk ( $\geq 0.056 \mu\text{m}$ ) mass concentration  
 1049 enrichment values due to the firework event; species are shown with enrichments  $\geq 1.9$ . Figure S5  
 1050 shows similar results for all other species.



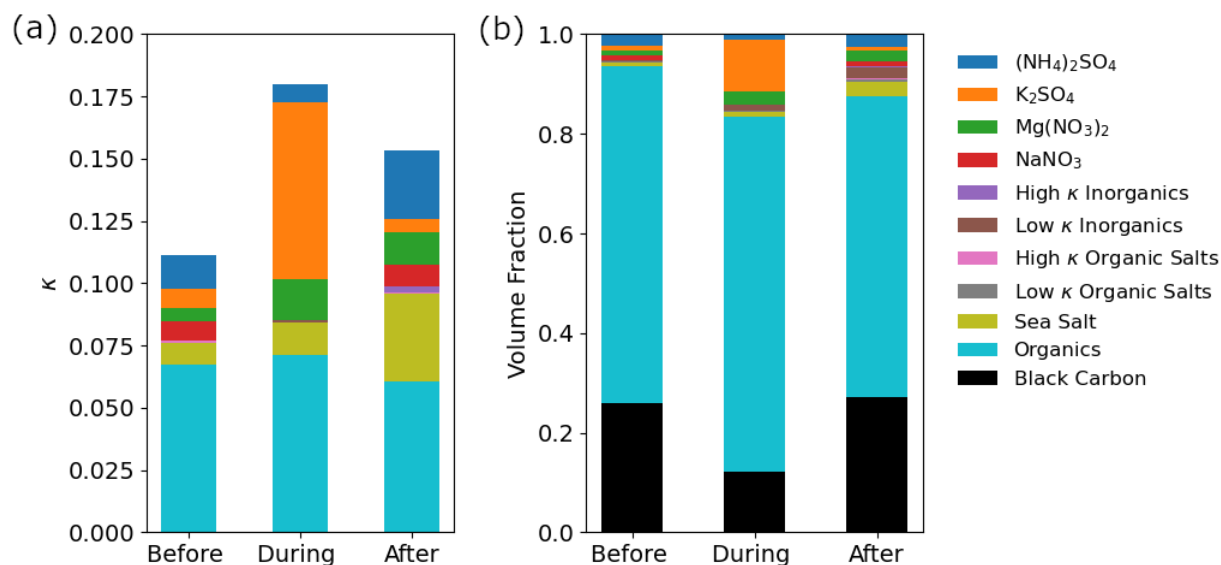


1051  
 1052 **Figure 6:** Size-resolved enrichments for individual firework tracer species in order of decreasing  
 1053 total bulk mass concentration enrichment (species from Fig. 5). Cut-point diameters with no  
 1054 valid data are left blank. The y-axis of Sr and Ba are truncated to more easily show enrichments  
 1055 in the larger size fractions. Figure S6 shows similar results for all other species.



1056

1057 **Figure 7:** Scanning electron microscope (SEM) images of (a) a blank PTFE (Teflon) substrate  
1058 and (b-f) particles in different diameter ranges with firework influence: (b) 0.1 – 0.18 μm, (c)  
1059 0.18 – 0.32 μm, (d) 0.32 – 0.56 μm, (e-f) 0.56 – 1.0 μm.



1060

1061 **Figure 8:** (a) Kappa ( $\kappa$ ) values for the aerosol fraction between 0.056 – 3.2  $\mu\text{m}$  before, during,  
 1062 and after the firework event. The speciated contributions to the overall  $\kappa$  values (represented by  
 1063 the colors) are categorized based on the classes of compounds in the legend following past work  
 1064 (AzadiAghdam et al., 2019). Ammonium sulfate,  $\text{K}_2\text{SO}_4$ ,  $\text{Mg}(\text{NO}_3)_2$ , and  $\text{NaNO}_3$  are high  $\kappa$   
 1065 inorganics but are plotted separately because of their large contributions. The speciated  
 1066 contributions were calculated by multiplying the (b) volume fraction of each compound class by  
 1067 its intrinsic  $\kappa$  value (Table S4).